AD-A190 861 DEFORMATION RIPPLE FROM THE SPLAT (SPRAY-LEAD-AT-TARGET) IMPULSE SIMULATION TECHNIQUE(U) APTEK INC SAN JOSE CA H E LINDBERG 03 NOV 87 A-86-7R 1/1

UNCLASSIFIED DNA-TR-86-361 DNA001-85-C-0264 F/G 19/9 NL

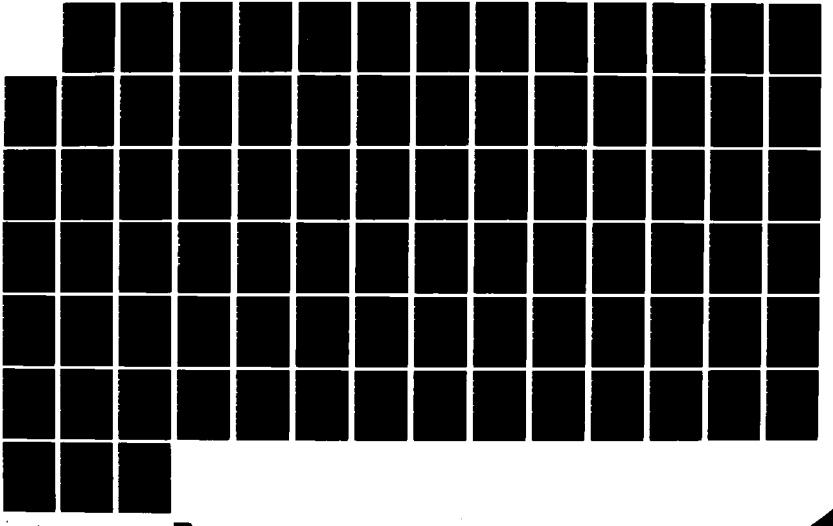

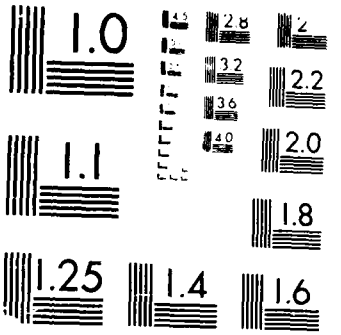

(4)

DNA-TR-86-361

DEFORMATION RIPPLE FROM THE SPLAT IMPULSE SIMULATION TECHNIQUE

H. E. Lindberg
APTEK, Inc.
4320 Stevens Creek Blvd.
Suite 145
San Jose, CA 95129

3 November 1987

Technical Report

CONTRACT No. DNA 001-85-C-0264

THIS WORK WAS SPONSORED BY THE DEFENSE NUCLEAR AGENCY
UNDER RDT&E RMC CODE B3460B5/642 RX RC 00017 25904D.

Prepared for
Director
DEFENSE NUCLEAR AGENCY
Washington, DC 20305-1000

Destroy this report when it is no longer needed. Do not return to sender.

PLEASE NOTIFY THE DEFENSE NUCLEAR AGENCY ATTN: TITL, WASHINGTON, DC 20305 1000, IF YOUR ADDRESS IS INCORRECT, IF YOU WISH IT DELETED FROM THE DISTRIBUTION LIST, OR IF THE ADDRESSEE IS NO LONGER EMPLOYED BY YOUR ORGANIZATION.

DISTRIBUTION LIST UPDATE

This mailer is provided to enable DNA to maintain current distribution lists for reports. We would appreciate your providing the requested information.

☐ Add the individual listed to your distribution list.

☐ Delete the cited organization/individual.

☐ Change of address.

NAME: _____

ORGANIZATION: _____

OLD ADDRESS	CURRENT ADDRESS
_____	_____
_____	_____
_____	_____

TELEPHONE NUMBER: (___) _____ _____

SUBJECT AREA(s) OF INTEREST:

_____ _____

_____ _____

_____ _____

DNA OR OTHER GOVERNMENT CONTRACT NUMBER: _____

CERTIFICATION OF NEED-TO-KNOW BY GOVERNMENT SPONSOR (if other than DNA):

SPONSORING ORGANIZATION: _____

CONTRACTING OFFICER OR REPRESENTATIVE: _____

SIGNATURE: _____

CUT HERE AND RETURN

Director
Defense Nuclear Agency
ATTN: [redacted] TITL
Washington, DC 20305-1000

Director
Defense Nuclear Agency
ATTN: [redacted] TITL
Washington, DC 20305-1000

UNCLASSIFIED
SECURITY CLASSIFICATION OF THIS PAGE

REPORT DOCUMENTATION PAGE

1a. REPORT SECURITY CLASSIFICATION UNCLASSIFIED	1b. RESTRICTIVE MARKINGS
2a. SECURITY CLASSIFICATION AUTHORITY N A since Unclassified	3. DISTRIBUTION / AVAILABILITY OF REPORT Approved for public release; distribution is unlimited.
2b. DECLASSIFICATION / DOWNGRADING SCHEDULE N A since Unclassified	
4. PERFORMING ORGANIZATION REPORT NUMBER(S) A-86-TR	5. MONITORING ORGANIZATION REPORT NUMBER(S) DNA-TR-86-361
6a. NAME OF PERFORMING ORGANIZATION APTEK, Inc 6b. OFFICE SYMBOL (If applicable)	7a. NAME OF MONITORING ORGANIZATION Director Defense Nuclear Agency
6c. ADDRESS (City, State, and ZIP Code) 4320 Stevens Creek Blvd. Suite 145 San Jose, CA 95129	7b. ADDRESS (City, State, and ZIP Code) Washington, DC 20305-1000
8a. NAME OF FUNDING / SPONSORING ORGANIZATION 8b. OFFICE SYMBOL (If applicable) SPAS/Frankel	9. PROCUREMENT INSTRUMENT IDENTIFICATION NUMBER DNA 001-85-C-0264
8c. ADDRESS (City, State, and ZIP Code)	10. SOURCE OF FUNDING NUMBERS PROGRAM ELEMENT NO. 62715H; PROJECT NO. RX; TASK NO RC; WORK UNIT ACCESSION NO DH200851

11. TITLE (All caps. Include Security Classification)
DEFORMATION RIPPLE FROM THE SPLAT IMPULSE SIMULATION TECHNIQUE

12. PERSONAL AUTHOR(S)
Lindberg, Herbert E.

13a. TYPE OF REPORT	13b. TIME COVERED	14. DATE OF REPORT (Year, Month, Day)	15. PAGE COUNT
Technical	FROM 851101 TO 860901	871103	82

16. SUPPLEMENTAL NOTATION
This work was sponsored by the Defense Nuclear Agency under RDT&E RMC Code B3460857642 RX RC 00017 25904D.

17. COSATI CODES		
FIELD	GROUP	SUB-GROUP
20	11	
13	13	

18. SUBJECT TERMS (Continue on reverse if necessary and identify by block number)
Buckling, Dynamic, Imperfections, Impulsive Load, Plates, Ripple, Shells, Simulation, Explosives

19. ABSTRACT (Continue on reverse if necessary and identify by block number)

Deformation rippling of plates and cylindrical shells loaded by the lead sprays from uniformly spaced strands of mild detonating fuse (MDF) is calculated by three methods to explore the nature of the ripple deformations and their influence on dynamic pulse buckling. The cyclic variations in loading from one strand position to the next in this spray-lead-at-target (SPLAT) impulse loading technique cause ripples in deformation by two basic mechanisms: variations in total accumulated impulse intensity from one location to another, and variations in the times at which impulse increments are delivered from one location to another.

20. DISTRIBUTION / AVAILABILITY OF ABSTRACT	21. ABSTRACT SECURITY CLASSIFICATION
☐ UNCLASSIFIED / UNLIMITED ☒ SAME AS RPT ☐ DTIC USERS	UNCLASSIFIED
22a. NAME OF RESPONSIBLE INDIVIDUAL Sandra E. Young	22b. TELEPHONE (Include Area Code) (202) 325-7042 22c. OFFICE SYMBOL DNA/CSTI

DD FORM 1473, 84 MAR

SECURITY CLASSIFICATION OF THIS PAGE
UNCLASSIFIED

19. ABSTRACT (Continued)

Target wall rippling caused by the former is called *impulse ripple*. Rippling caused by the latter is called *deformation ripple*, because differential impulse delivery times produce a change in deformation from one point to another even if the total accumulated impulse is essentially uniform. Impulse ripple was analyzed in detail by Murray and Lindberg; the present report concentrates on deformation ripple, for cases in which the impulse ripple is essentially zero.

In the first analytical method, the bending stiffness of the target wall is neglected, which gives quite general results (a minimum number of parameters) that are valid for early motion and demonstrate the fundamental mechanisms of deformation ripple. In the second analytical method, bending stiffness and vibrations are included but not in-plane thrust. Solutions are obtained by Fourier cosine transforms. It is found that the bending vibrations sustain the ripple motion at higher amplitudes to later times than without vibrations.

In the third analytical method, bending stiffness, in-plane thrust and elastic-plastic material behavior are all included. Solutions are obtained with the DYNA2D finite element code. It is found that the rippling leads to dynamic pulse buckling for shell and SPLAT parameters in some of the thin shell, low impulse experiments performed at SRI International. The thinness of the shells makes them susceptible to bending and buckling, and the low impulse intensity requires wide spacing of the MDF strands and hence gives rise to substantial deformation ripple. It remains to determine whether natural shell and loading imperfections dominate over these SPLAT ripples for most practical cases of interest.

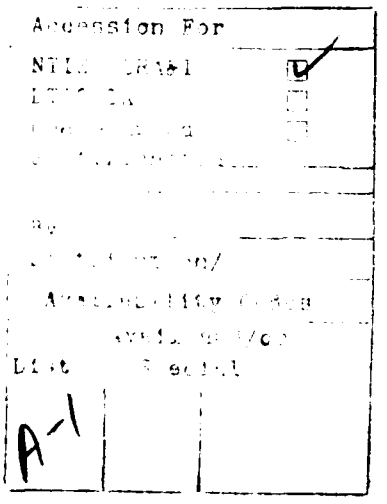

TABLE OF CONTENTS

LIST OF ILLUSTRATIONS

SECTION 1
INTRODUCTION

In the spray lead at target (SPLAT) technique, impulse is produced by the spray of lead from strands of mild detonating fuse (MDF) exploded above the target surface. An end-on view of the MDF strands and target for the simplest case of uniform impulse on a flat target is given in Figure 1. In Reference 1 it is shown that satisfactory smoothness of the resulting impulse distribution depends on the ratio $S_r = S/D$, where S is the standoff of the MDF strands from the target surface and D is the spacing between strands. If this ratio is greater than about 1.4, the ripple in impulse intensity from strand to strand is about 0.25% of the average impulse intensity.

The design rule for strand standoff is therefore such that S_r is always greater than about 1.4. As the strands are separated farther apart to reduce the impulse intensity, for example in producing a cosine distribution of impulse on a target of circular section, the strands are also placed farther from the target to maintain this minimum allowable standoff-to-spacing ratio. This sets a lower limit on impulse intensity for a given MDF size and target diameter: as the standoff becomes an appreciable fraction of the target diameter, it is no longer possible to accurately tailor the impulse intensity to the desired distribution.

This procedure is simple and straight forward and allows design of strand distributions independent of the nature of the target and its response. However, in a more detailed analysis of impulse delivery by MDF, also given in Reference 1, it is shown that the impulse at any point on the target is delivered as a sequence of loading bursts as the sprays arrive from individual MDF strands. Most of the impulse comes from the seven strands nearest each point. The time required for these loading bursts to accumulate to the total impulse intensity is directly proportional to the strand standoff and inversely proportional to the lead spray velocity (which

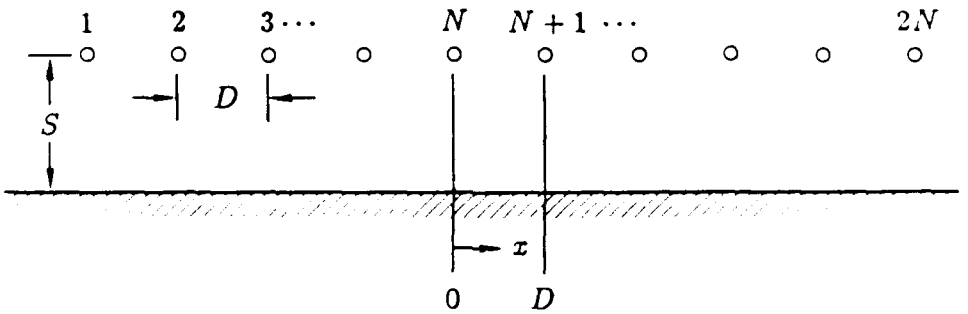

Figure 1. Uniform array of MDF strands above a flat target.

is 0.7 mm/μs for commercial mild detonating fuse). For uniform impulse on a flat target, Figure 3.13 in Reference 1 shows that for a standoff of 50 mm, 90% of the impulse is delivered by 100 μs and 96% is delivered by 200 μs. These times also set a limit on the maximum allowable standoff for a given target, since the impulse delivery time must be short compared with structural response times of interest.

Delivery of impulse by a sequence of bursts also introduces another form of ripple. This ripple is more difficult to generalize than the ripple in total accumulated impulse intensity because it depends on the particular structure being loaded. With finite times between impulse bursts that are different for different positions on the target relative to the strand positions, even with a uniform accumulated impulse the target is left with a displacement ripple because of target motion between impulse bursts. It is shown in this report that this ripple persists even as the standoff-to-spacing ratio S_r is increased substantially above the value 1.4 for reasonably uniform impulse intensity.

We first consider target response for impulse delivery times that are short compared with the periods of target bending response, which is the desired situation for impulse simulation. Then target deformation during impulse delivery can be calculated by considering only the target mass and not its stiffness or strength. These calculations show the persistance of deformation ripple even for rather large values of S_r. Derivation of the equations of motion for this simple case are given in Section 2. Example results for a representative target of interest are given in Section 3.

The results in Section 3 show than for very thin shell targets, which are the targets for which SPLAT finds its principal use, ripple response amplitudes are large enough to cause concern for simulation of dynamic pulse buckling. However, as the target wall becomes thicker, it is necessary to include the stiffness and hence dynamic response of the target in calculating the deformation ripple. Finite Fourier transforms are used in Section 4 to calculate this response. A few representative results are presented, along with a computer program that can be used to guide the design of MDF arrays to maintain deformation ripple at a satisfactorily small value compared with natural shell imperfections.

At early times the deformation ripple with the target wall stiffness included in the calculations has features similar to those for the zero stiffness approximation. However, the maximum ripple occurs at later times, while the target is responding by elastic vibrations. Thus, the amount of ripple is only indicative of the equivalent initial imperfection to be applied in a more complete response calculation with in-plane forces included as well as bending stiffness. Therefore, in Section 5 we calculate complete elastic-plastic response of a representative shell, including in-plane forces that lead to dynamic pulse buckling. This response is compared with response calculated in Section 4, with bending but not buckling, as an example of how the much simpler Fourier transform calculation can be used to estimate equivalent imperfections for buckling.

SECTION 2
THEORY OF DEFORMATION RIPPLE FOR EARLY TIMES

2.1 Impulse Ripple.

The equations needed to calculate deformation ripple include those needed for impulse ripple, so we start by calculating the impulse ripple. Consider a uniform array of strands at spacing D and standoff S above a flat target as shown in Figure 1. Impulse intensity is calculated by assuming the lead spray and impact mechanics depicted in Figure 2. The lead from each strand is assumed to expand at uniform velocity v in a circular arc unimpeded by the expansion of lead from neighboring strands. When this arc intersects the target surface, the velocity of the lead normal to the target is assumed to come to zero with no rebound.

Experimental results given in Reference 1 show that the actual normal impulse intensity is about 30% greater than the impulse calculated with this assumption, presumably because of some rebound and because of impulse delivered by the explosive gas, which is neglected here. To account for this difference, the mass m of the MDF per unit length is increased above its actual value by 30%. The same experiments demonstrated that impulse delivered tangential to the target surface is essentially zero, leading to the assumption that the lead moves tangentially to each impact point after impact.

The radial momentum of an element of lead of arc length $d\theta$ from a single strand is

$$dM = \frac{m}{2\pi}\, d\theta \cdot v \tag{1}$$

All the lead in the lower semicircle impacts a flat target of infinite extent. The total momentum normal to the target surface from a single strand is therefore

$$I_{NT} = \int_{-\pi/2}^{\pi/2} \frac{m\, d\theta}{2\pi} \cdot v \cos\theta = \frac{mv}{\pi} \tag{2}$$

The impulse intensity for an infinite array of uniformly spaced strands can be found by calculating the total momentum from N such strands and dividing by the length L spanned by these strands.

$$I_\infty = \frac{N I_{NT}}{L} = \frac{mv}{\pi}\frac{N}{L} = \frac{mv}{\pi D} \tag{3}$$

In the final expression, we have used $D = L/N$.

To calculate the impulse intensity distribution from a single strand, we again use the elemental momentum of an arc length $d\theta$ as given in Eq. (1) but consider

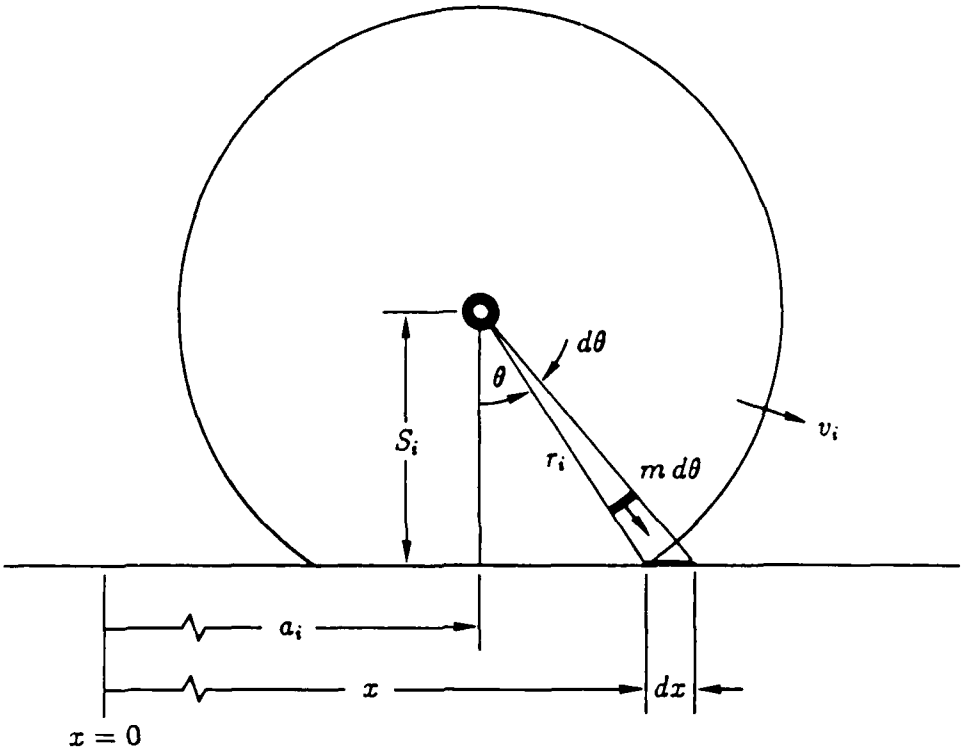

Figure 2. Lead spray geometry for the i^{th} strand.

in more detail that the arc element impacts the target in a corresponding length dx along the target surface. From the geometry in Figure 2, this length is

$$dx = \frac{r\,d\theta}{\cos\theta} = \frac{S\,d\theta}{\cos^2\theta} \tag{4}$$

in which r is the distance from the MDF strand to the point of impact, x is the coordinate of this point, S is the standoff of the strand from the target, and θ is the angle between the normal to the surface and the radius vector r.

With the assumption that the lead comes completely to rest upon impact, the impulse intensity delivered to the target at location x is found by dividing the momentum of the lead element by the area over which it impacts, with the result

$$I(x) = \frac{mv}{2\pi S}\cos^2\theta \tag{5}$$

The impulse intensity normal to the target surface is found by multiplying the total impulse intensity by $\cos\theta$.

$$I_N(x) = \frac{mv}{2\pi S}\cos^3\theta \tag{6}$$

The impulse intensity tangential to the target surface with this ideal inelastic impact assumption is found by multiplying the total impulse intensity by $\sin\theta$. For an

assumption of zero velocity change tangential to the surface, the tangential impulse intensity is zero, in better agreement with the experimental results in Reference 1.

For the i^{th} strand in an arbitrarily arranged array we have

$$\cos\theta_i = \frac{S}{r_i} \tag{7}$$

and

$$r_i(x) = \left[(x - a_i)^2 + S_i^2\right]^{1/2} \tag{8}$$

in which a_i is the position of the strand measured from the x origin. The total impulse from N strands, from Eqs. (6) and (7), is

$$I_{NT} = \sum_{i=1}^{N} \frac{m_i v_i}{2\pi S_i} \left(\frac{S_i}{r_i}\right)^3 \tag{9}$$

The impulse ripple is defined in Reference 1 as the difference in impulse intensity at points directly under and midway between two strands, in a uniform array with standoff S and spacing D, devided by the infinite array impulse intensity given by Eq. (3). With the origin for x taken at a position directly under the central strand of an array of $2N + 1$ strands, the impulse ripple between this point and the point midway to the next strand is

$$R(S_r) = \frac{S_r^2}{2} \sum_{i=-N}^{N} \left\{(i^2 + S_r^2)^{-3/2} - \left[(\frac{1}{2} + i)^2 + S_r^2\right]^{-3/2}\right\} \tag{10}$$

where

$$S_r = S/D \tag{11}$$

Note that this coordinate system, used in Reference 1, is different from the coordinate system in Figure 1, which is more convenient in the present work.

Values of ripple ratio from this equation for several values of N and for $S_r = S/D$ ranging from 1.0 to 2.5 are given in Table 1. For large values of N, the ripple is less than 0.25% for $S_r > 1.4$. Note that at large values of S_r, the ripple is reduced substantially below this value only for large values of N. For example, with 11 strands ($N = 5$), the ripple *increases* as S_r is increased above 1.9. Thus, ripples less than about 0.25% require very large arrays. We show later in this section that the impulse delivery times for these last increments in impulse, from the outer strands of large arrays, become impractically long and hence ripples smaller than about 0.25% are virtually unobtainable in practice.

However, an impulse ripple of 0.25% is quite satisfactory for most applications. The corresponding deformation ripple, neglecting the strength of the target during the short impulse delivery time, is

$$y_{rip} = VRt \tag{12}$$

Table 1. Percent impulse ripple for various strand standoff ratios and numbers of strands.

S/D	*Total Number of Strands,* $2N+1$				
	11	17	21	31	41
1.00	2.5179	2.4875	2.4836	2.4812	2.4808
1.10	1.4258	1.3897	1.3850	1.3822	1.3817
1.20	0.8186	0.7765	0.7710	0.7676	0.7670
1.30	0.4840	0.4357	0.4293	0.4253	0.4246
1.40	0.3021	0.2473	0.2400	0.2354	0.2346
1.50	0.2052	0.1439	0.1356	0.1304	0.1285
1.60	0.1556	0.0877	0.0783	0.0725	0.0714
1.70	0.1322	0.0576	0.0472	0.0407	0.0395
1.80	0.1232	0.0421	0.0306	0.0233	0.0220
1.90	0.1222	0.0345	0.0219	0.0139	0.0124
2.00	0.1254	0.0314	0.0176	0.0089	0.0072
2.10	0.1309	0.0307	0.0158	0.0062	0.0044
2.20	0.1375	0.0313	0.0153	0.0049	0.0029
2.30	0.1447	0.0327	0.0155	0.0043	0.0021
2.40	0.1520	0.0346	0.0162	0.0041	0.0017
2.50	0.1592	0.0366	0.0170	0.0041	0.0016

where V is the target wall velocity from the uniform impulse given by Eq. (3), R is the ripple ratio from Eq. (10) and t is time. Consider an example in which this velocity just produces hoop yield in a circular target under symmetric radial impulse. Then

$$V = c\epsilon_y = (5\text{mm}/\mu\text{s})(0.004) = 0.02\text{mm}/\mu\text{s} \tag{13}$$

where c is the velocity of elastic membrane waves in the shell wall and ϵ_y is material yield strain. The numerical values are for aluminum 6061-T6 alloy. Wall motion during a 50 μs impulse delivery time is then

$$\frac{y_{\text{rip}}}{h} = \frac{(0.02\text{mm}/\mu\text{s})(50\mu\text{s})R}{h} = \frac{R}{h}\,, \qquad h \text{ in mm} \tag{14}$$

in which h is wall thickness.

Thus, for a 1-mm-thick target wall, the deformation ripple as a fraction of the wall thickness is equal to the normalized impulse ripple given by Eq. (10). A deformation ripple of 0.25% of the wall thickness is generally quite acceptable.

2.2 Deformation Ripple.

The radius of the lead spray from each MDF strand in a uniform array expands at constant velocity v according to

$$r_i = S + vt \tag{15}$$

where time t is defined such that the spray from each and every strand begins to impact the target surface at $t = 0$. After this initial impact just opposite each strand, the impact points from each strand sweep across the target as a pair of loads running in opposite directions. Each point on the target surface receives a single impulse burst from each strand; strands to the left of the point deliver impulse by right-running impacts and strands to the right of the point deliver impulse by left-running impacts. In either case, the time of impact at location x from the i^{th} strand is

$$t_i(x) = \frac{r_i(x) - S}{v} \tag{16}$$

where $r_i(x)$ is given by Eq. (8). In Reference 1 the time history of impulse delivery was calculated for lead sprays expanding in finite thickness shells of lead particles. However, it was found that the most important time feature of loading was the traveling load feature just described. The finite time loading of each impulse burst was found to be small compared with the overall impulse delivery time from the several strands that delivered significant impulse. Thus, the present calculations are simplified by assuming zero-thickness lead shells as indicated in Figure 2.

If the impulse delivery time is short compared with structural response times of concern, target motion can be calculated by considering only the mass of the target, which is taken here as a shell of constant areal density ρh, where ρ is structure material density and h is wall thickness. The impulse burst I_i from the i^{th} strand therefore results in a velocity increment that can be integrated immediately to obtain a displacement contribution given by

$$y_i(x) = \begin{cases} 0 & t < 0 \\ (t - t_i) I_i(x)/\rho h & t > 0 \end{cases} \tag{17}$$

The total motion from N strands is then

$$y(x,t) = \frac{mvS^2}{2\pi\rho h} \sum_{i=1}^{N} \left[\frac{1}{r_i^3(x)} (t - t_i) H(t - t_i) \right] \tag{18}$$

where $I_i(x)$ has been taken from Eq. (6) and $H(t)$ is the Heaviside step function,

$$H(t) = \begin{cases} 0 & t < 0 \\ 1 & t \geq 0 \end{cases} \tag{19}$$

It is convenient to express Eq. (18) in terms of the velocity V that would be imparted to the target wall by an infinite array, so that with Eq. (3) we have

$$V = \frac{I_\infty}{\rho h} = \frac{mv}{\pi D \rho h} \tag{20}$$

The coefficient in Eq. (18) is then expressed as

$$\frac{mvS^2}{2\pi\rho h} = \frac{VDS^2}{2} \tag{21}$$

For the examples to be considered in the following sections, we consider an array of $2N$ strands as indicated in Figure 1. Ripple deformations and structural response are calculated for a section of structure extending from strand N to strand $N+1$ at the center of this array, as shown in the figure for $N = 5$. Then the strand locations in a coordinate system with its origin at the N^{th} strand is

$$a_i = (i - N)D \tag{22}$$

An explicit expression for deformation ripple is not given because the deformation ripple patterns are much more complex than the impulse ripple patterns. The peaks and valleys of the impulse ripple are always aligned with locations directly under and between MDF strands, respectively. We will see in the next section that the deformation ripple sometimes has peaks and valleys aligned in this way, but just as often the deformation ripple has peaks located off center and the ripple wavelength is shorter than the strand spacing.

SECTION 3
EXAMPLE DEFORMATION RIPPLES

3.1 Example Specification and Analysis Applicability.

We consider a long, thin cylindrical shell of aluminum 6061-T6 alloy under symmetric radial impulse. The shell diameter is 16 inches (406 mm) and its wall thickness is 30 mils (0.762 mm). In the present section we calculate motion for times short enough that only the mass of the shell is important in its response, as discussed earlier, and further idealize the loading and early-time response as that of a flat sheet loaded by a uniformly spaced array of MDF strands as indicated in Figure 1. The impulse intensity is 800 taps, which is a level that results in moderate dynamic pulse buckling when the full response is calculated.

The reasonableness of these idealizations is indicated by the periods of structural modes of concern compared with the duration of early time response under consideration. Neglect of the wall bending stiffness and in-plane buckling forces is reasonable only if the periods of shell response modes are long compared with the impulse delivery times under consideration. The period of the elastic hoop mode is $2\pi a/c = 255\mu$s, where a is the shell radius and c is elastic membrane wave velocity. Threshold pulse buckling in this shell, with radius-to-thickness ratio $a/h = 267$, reaches its peak deformation at a time equal to about half this period, or at about 125 μs. Buckling motion can therefore be neglected for times less than about 60 μs.

The strand spacing for an impulse of 800 taps with 2 gr/ft MDF is $D = 26$ mm. The period of bending oscillations of a shell (or flat plate) at this wavelength is $0.552\ D^2/hc$, where h is wall thickness. For the shell here, this period is 98 μs. Response at this wavelength for times short compared with a quarter period (less than about 20 μs) will depend mainly on the mass of the shell and not its bending stiffness. Higher harmonics have shorter periods, inversely in proportion to the square of the wavelength. Thus, motion in these higher harmonics cannot be calculated by neglecting bending stiffness as done in this chapter. We will see in the following results that these harmonics are excited, but since the associated periods are comparable to or shorter than the impulse delivery times, the present results indicate only the presence of the excitation and not the resulting amplitude. Response with bending stiffness, and hence with bending vibration, included in the analysis is given in Section 4. Complete response, with buckling as well as bending vibrations, is calculated in Section 5.

3.2 Nature of Wall Motion.

All of the calculations were made with 16 strands in an array with a separation distance of $D = 26$ mm. The corresponding late-time wall velocity is 0.0384 mm/μs. Figure 3 gives plots of deformation versus time during early motion for a standoff ratio $S_r = 1.0$. Curves are given for $x/D = 0$, 0.3, and 0.5, which from Figure 1 correspond to locations directly under a strand, some distance from a strand, and midway between two strands, respectively.

The most apparent observation is that the point midway between strands does not begin to move until about 4 μs after initial motion of the point directly under a strand, because of the larger distance from the closest strand to this point. (The two bends in the curve at 4 and 5 μs, for the midway point, is an artifice of the finite times at which deformation was calculated. The actual impact time is 4.38 μs.) As a result, a gap of motion opens up between the two points.

When the midway point begins to move, it has a higher initial velocity than the point under a strand because it receives impulse from two opposing strands, at $x/D = 0$ and 1. The gap in motion between the two points therefore begins to close. At 14 μs the two curves intersect. Then at about 15 μs the point under a strand receives impulse from the next opposing pair of strands, at $x/D = -1$, 2, and attains a velocity higher than the current velocity of the midway point. A gap in motion therefore begins to open up once again. Motion of the $x/D = 0.3$ point falls between the motion of these two points. The slopes of the lines at the end of the plot are all less than the infinite array velocity 0.0384 mm/μs because by 30 μs impulse has been received only from the four strands closest to the $x/D = 0, 1$ interval.

In Figure 3(b) the same data as in Figure 3(a) are plotted but with motion measured relative to the motion of the point $x/D = 0$, under a strand. Also, curves for the points $x/D = 0.2$ and 0.4 have been added without confusion in this amplified version. The opening and closing of the relative motions is more apparent in this plot, as is the amplitude of deformation. The changes in relative velocity are sudden and quite large, because of the nature of SPLAT loading. They are not the result of calculating response at 1 μs time increments.

The same data are plotted in Figure 4 as a sequence of snapshots of the deforming shape at 5 μs time increments. For clarity, the shapes are again plotted relative to the locations directly under MDF strands, at $x/D = 0$ and 1. In this plot, the increasing and decreasing deformations must be observed by noting that the curves move up and down as one follows the time increments in sequence. For most of the time the dominant shape is approximately a sine wave with wavelength D. However, at the intermediate time $t = 15$ μs there are two waves within the length D. Thus, the modes excited by deformation ripple are more complex than for impulse ripple.

Figure 5(a) is a plot of relative deformation versus time similar to that in Figure 3(b) but extended to 100 μs. Over this longer duration the trend is for the

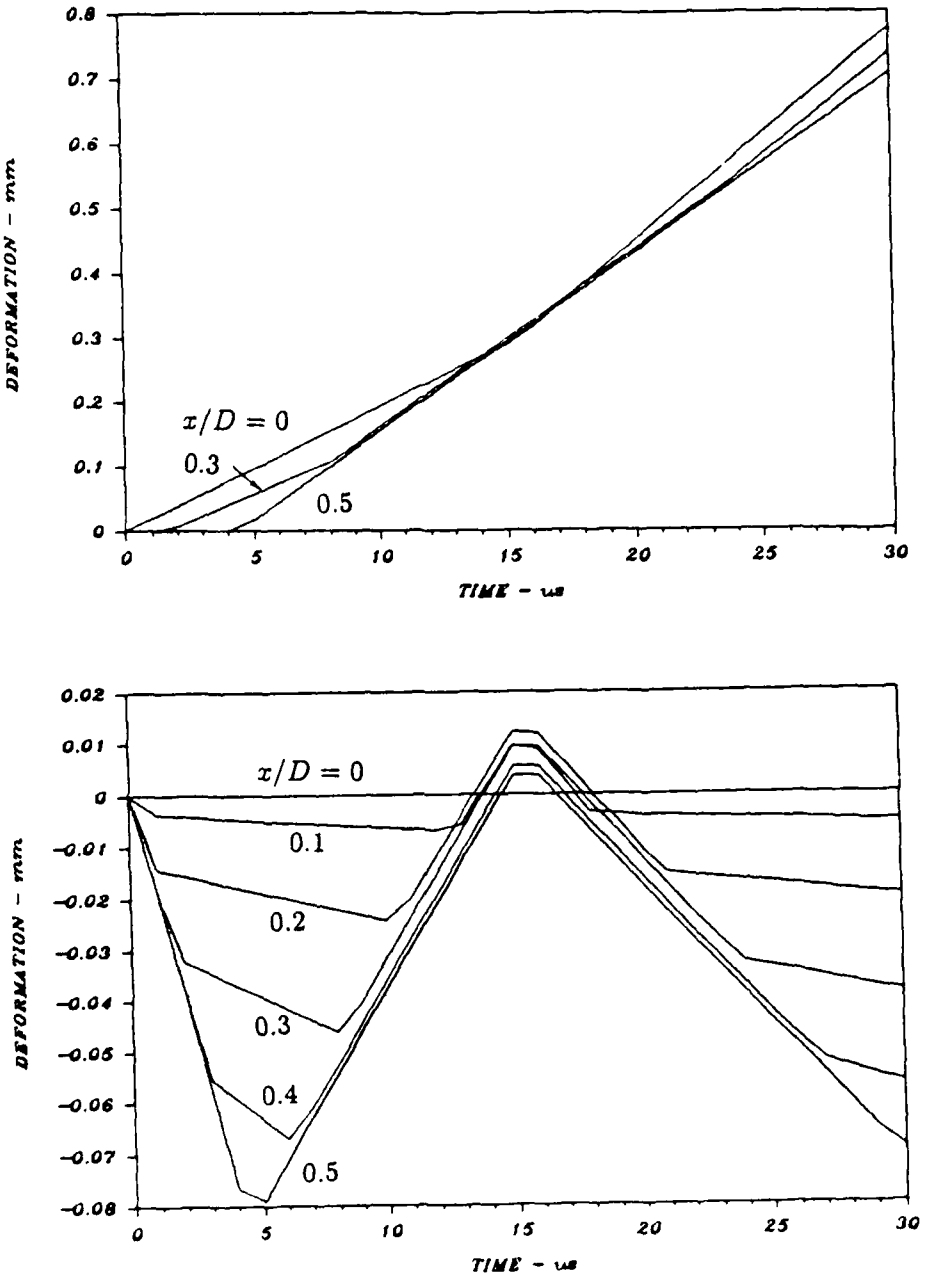

Figure 3. Total and relative deformation *vs.* time for $S_r = 1$.

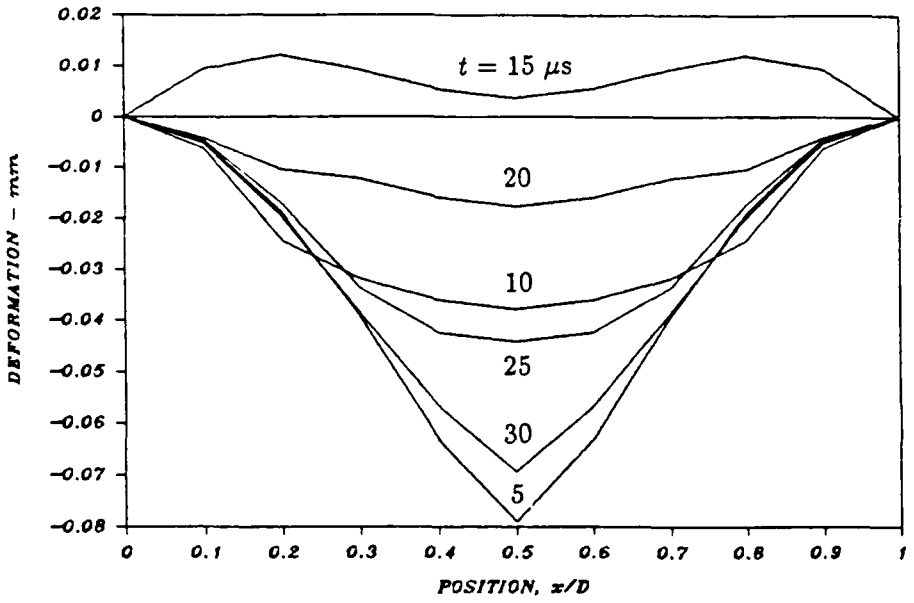

Figure 4. Strand-to-strand target shape at a sequence of times for $S_r = 1$.

amplitude of the oscillatory component of deformation to decrease with time. At late times the deformation increases steadily with time. This steady increase is the result of the impulse ripple, which leaves each point with a late-time relative velocity. The time increments were made coarser than in Figure 3 for convenience in using data point symbols in these plots, but are short enough to show the pertinent features of motion.

Figure 5(b) is a similar plot for the same strand spacing D but with the standoff increased such that $S_r = 1.6$. The most apparent result of this increase is that the late-time relative velocities do not approach steady values as they do for $S_r = 1.0$ in Figure 5(a). This is consistent with the very small impulse ripple for $S_r = 1.6$ as already observed in Table 2.1. The other important result of this increase is that the deformation ripple from differential impact times is smaller than in Figure 5(a). The maximum value is about 0.03 mm as compared with 0.08 mm for $S_r = 1$. However, the decrease expressed as a ratio is not falling nearly as rapidly as the decrease in impulse ripple given in Table 2.1. Thus, deformation ripple persists even as the impulse ripple falls to negligibly small values. Further examples of this persistance are given in the following paragraphs.

3.3 Effect of Standoff-to-Spacing Ratio on Deformation Ripple.

The above example shows that, while increasing S_r does not decrease the deformation ripple as rapidly as it does the impulse ripple, the decrease is nevertheless

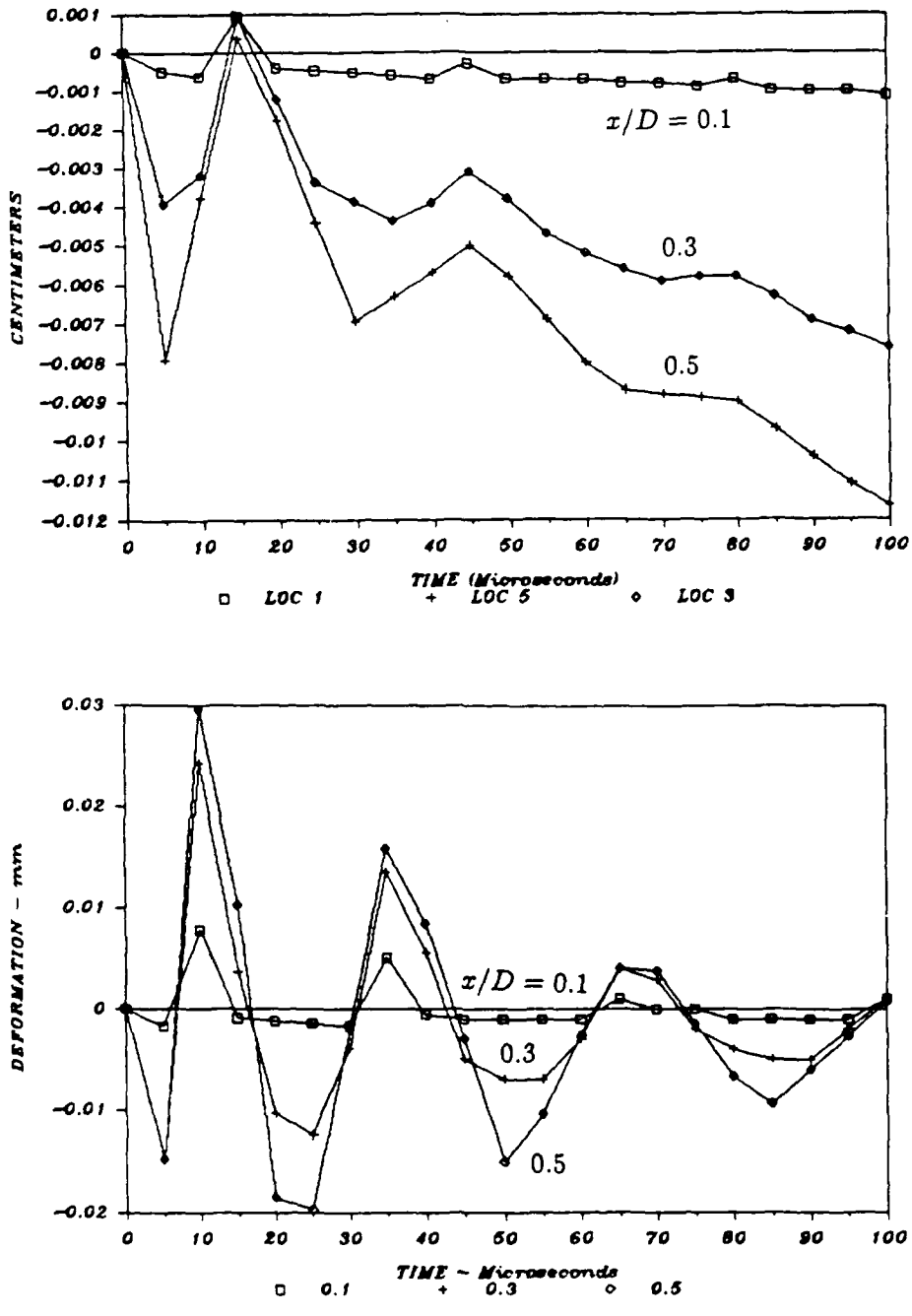

Figure 5. Relative deformation *vs.* time for $S_r = 1$ and $S_r = 1.6$.

substantial and forms the basis for obtaining satisfactorily smooth motion for impulse simulation with SPLAT. Also, for some applications, the MDF strands are placed at an angle to the target in order to obtain more nearly simultaneous impact. In recent experiments performed at SRI International (Reference 2), the strands were tilted from the axis of a cylindrical shell with dimensions as in the example here. The tangent of the tilt angle for simultaneous impact is v/v_d, where v is the lead particle velocity and v_d is the detonation velocity of the MDF. For commercial MDF, $v/v_d = (0.7\ \text{mm}/\mu\text{s})/(7\ \text{mm}/\mu\text{s}) = 0.1$. Thus, for a 260-mm strand length with $D = 26$ mm, S_r changes by one unit from one end of the strand to the other. In the following examples we change S_r from 1.0 to 2.0, which spans a range of practical interest where ripple is being minimized without excessive standoffs.

In Figures 6 through 14 we give plots of strand-to-strand deformation shape for this range in S_r. The plots are given at a sequence of times with S_r as a parameter in each plot. This method is used because each figure can then be visualized as series of sections through the deformed shell between strands that are tilted into the paper. This shows a second advantage of tilting the strands; the deformation ripple at each position along the length of the shell is different. This introduces twisting that resists buckling along the shell length.

In each figure, the deformation ordinates are given in absolute form but the graph is allowed to seek its maximum allowable scale, with the origin biased progressively farther from zero as time increases from figure to figure. Nevertheless, the vertical scale factor decreases somewhat from figure to figure. For convenience in comparing the figures, a vertical bar is drawn at the right side in each figure with a length corresponding to 0.1 mm at the scale of the figure. The bars change length appreciably only at late times.

The figures show a general decrease of the deformation ripple with increasing S_r and increasing time. Also, the shapes of the deformations change as these two parameters change. In fact, there is so much change that it is difficult to make general observations about the motion as it proceeds. The overall impression is that the deformations are complex and reasonably small, a combination that tends to inhibit initiation of pulse buckling from the nonuniformity in loading.

This same information is plotted in Figures 15 through 20 as plots of relative deformation versus position x/D at fixed S_r, with time as the parameter. Again, the most striking observation is the complexity of the motion. An interesting quantitative observation is the maximum peak-to-peak deformation in each plot expressed as a fraction of the shell wall thickness. These are given in each figure and range from 10.5% for $S_r = 1$ to 3.3% for $S_r = 2$.

Another form of presentation that gives more quantitative information is plots of relative deformation versus time, given in Figures 21 through 26. In these plots, position x/D is the parameter, as in Figures 3 and 5, which were used to introduce the features of motion. The monotonic but not dramatic decrease in deformation

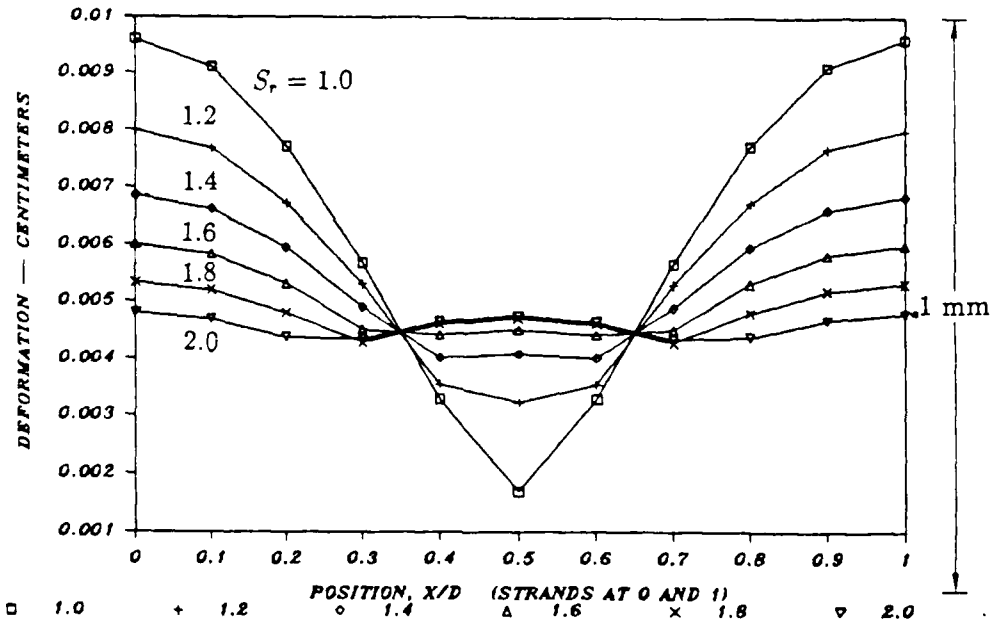

Figure 6. Strand-to-strand total deformation shapes at 5 μs for a sequence of S_r values.

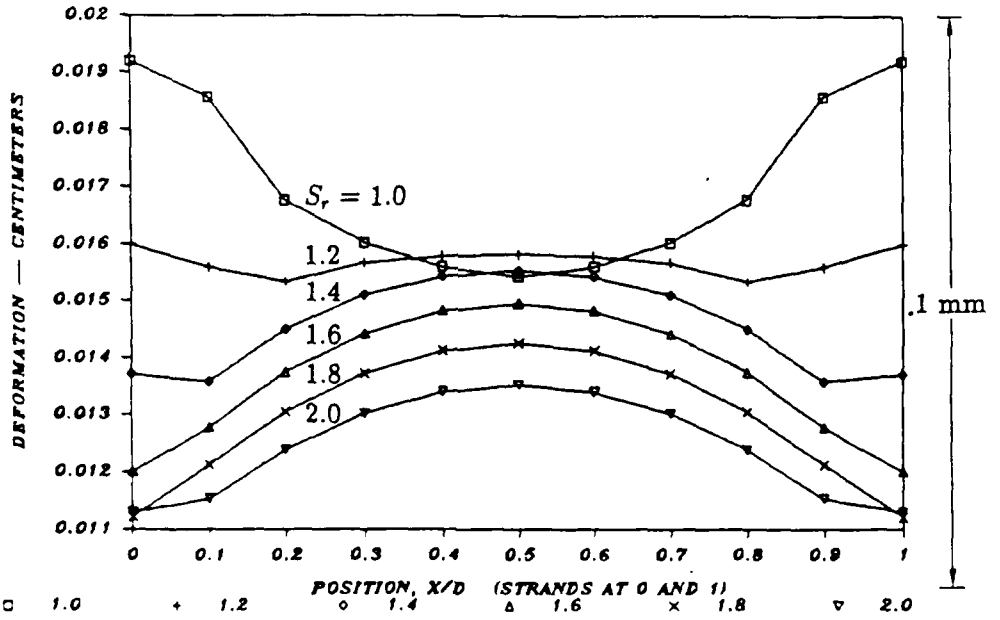

Figure 7. Strand-to-strand total deformation shapes at 10 μs for a sequence of S_r values.

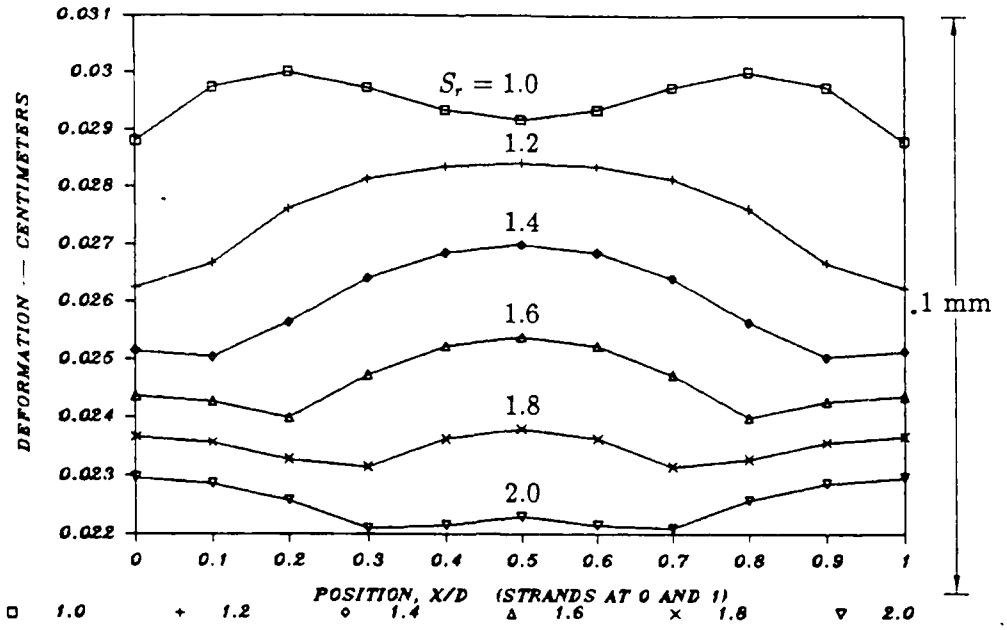

Figure 8. Strand-to-strand total deformation shapes at 15 μs for a sequence of S_r values.

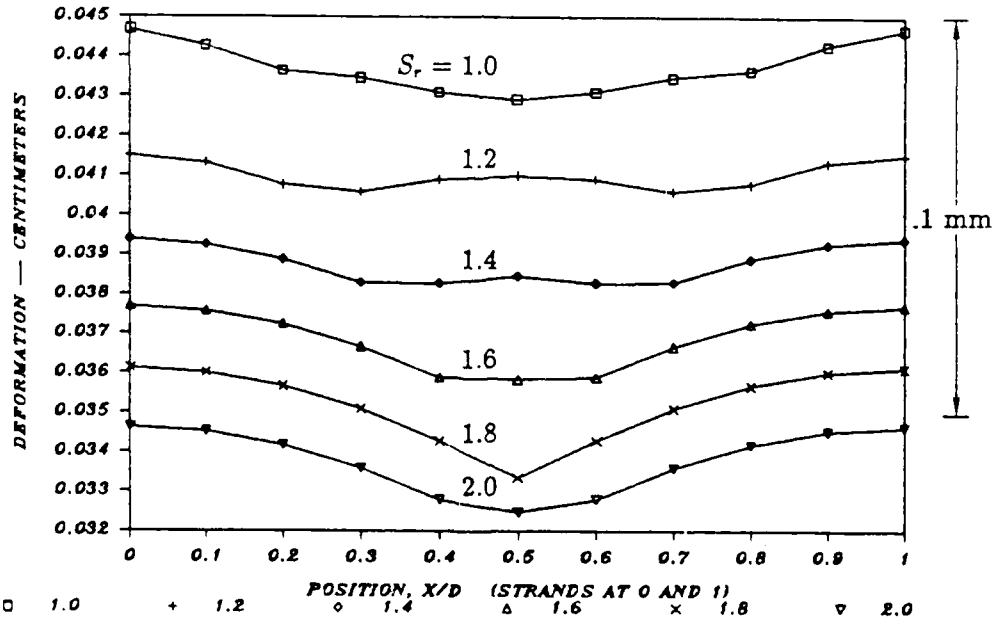

Figure 9. Strand-to-strand total deformation shapes at 20 μs for a sequence of S_r values.

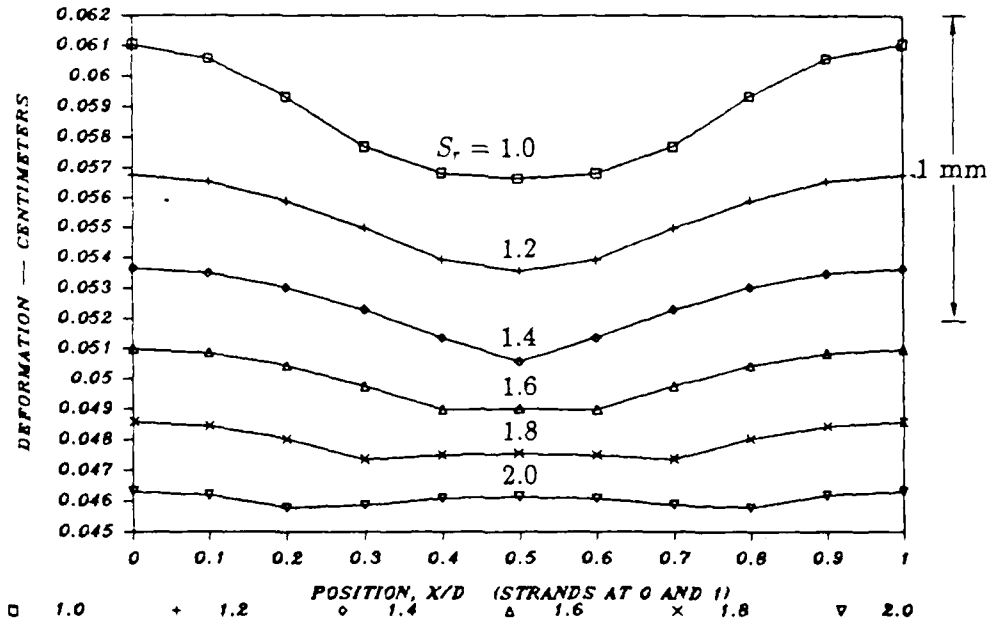

Figure 10. Strand-to-strand total deformation shapes at 25 μs for a sequence of S_r values.

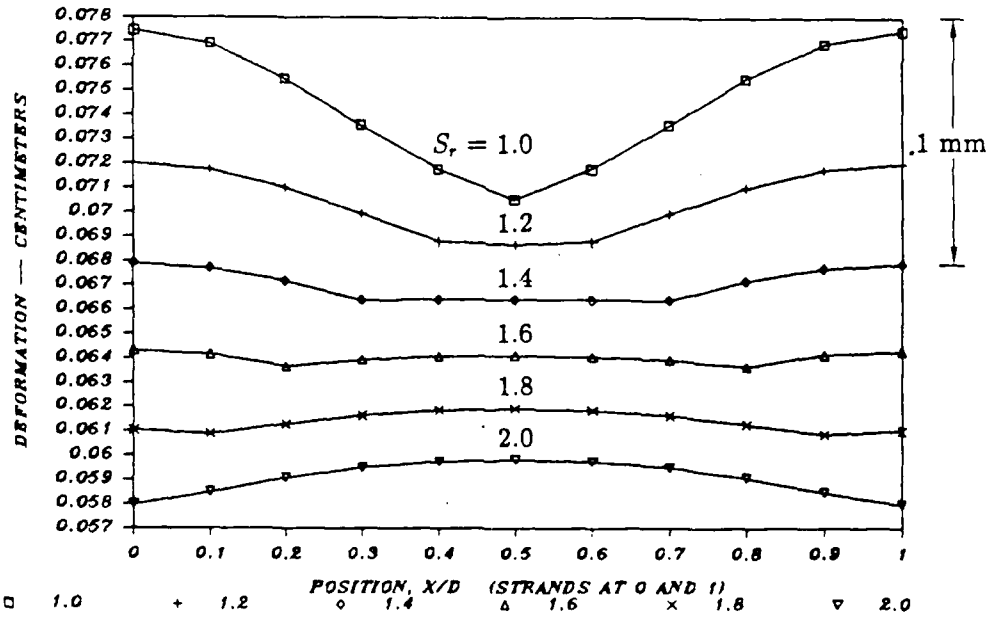

Figure 11. Strand-to-strand total deformation shapes at 30 μs for a sequence of S_r values.

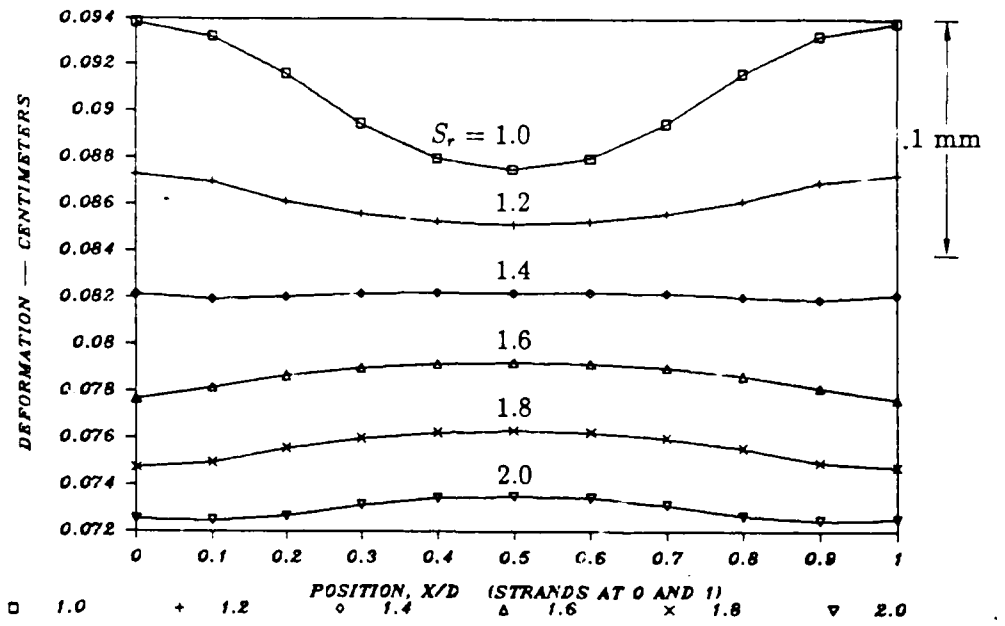

Figure 12. Strand-to-strand total deformation shapes at 35 μs for a sequence of S_r values.

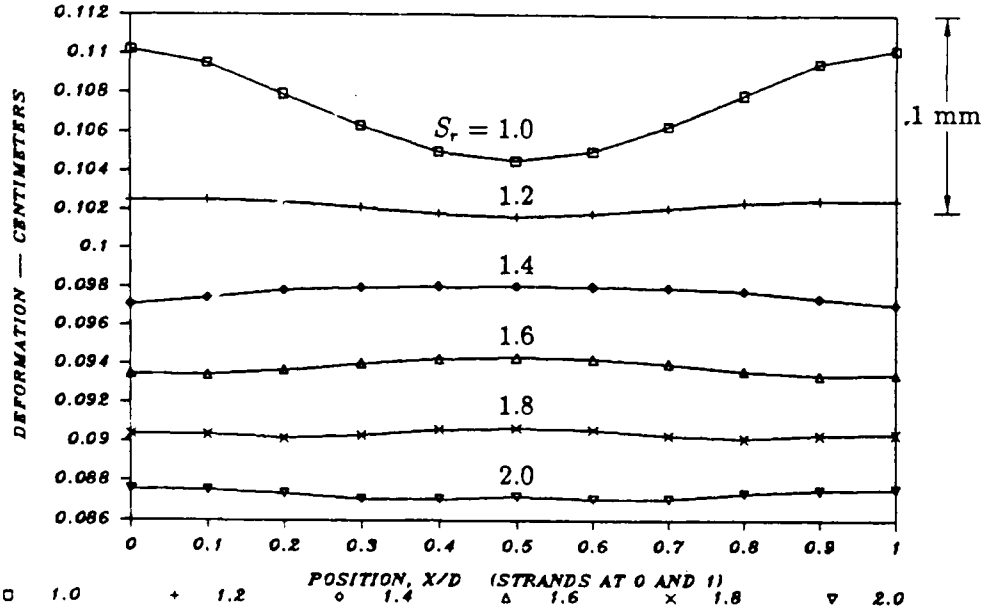

Figure 13. Strand-to-strand total deformation shapes at 40 μs for a sequence of S_r values.

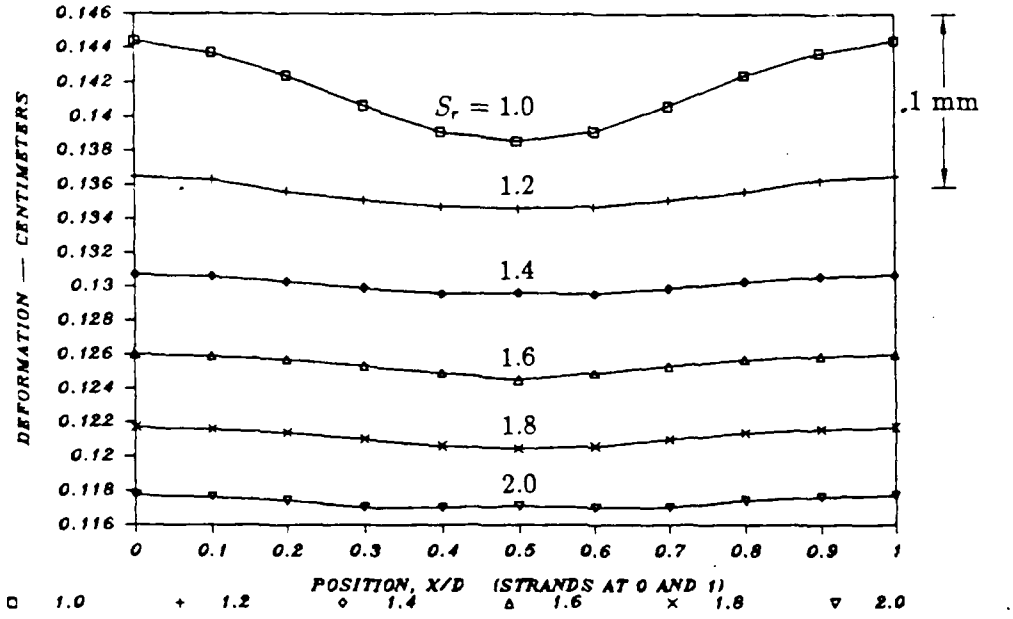

Figure 14. Strand-to-strand total deformation shapes at 50 μs for a sequence of S_r values.

amplitudes with increasing S_r is apparent. Also, the times at which the deformations reach their maxima are apparent, as is the observation that at the maxima the shapes tend to be their simplest, consisting essentially of a single wave of length D. The complex shapes with more than one wave in the MDF strand separation distance occur as the continuing SPLAT impacts straighten out the shell on its way to a maximum in the opposite direction.

The final observation is the slight decrease in the period of the deformation oscillations as S_r increases. The periods measured between the occurances of the positive going peaks in each of Figures 21 through 26 range only from 28 μs for $S_r = 1.2$ to 23 μs for $S_r = 2.0$. Thus, if this period excites a resonance when the actual stiffness of structural response is included in the analysis, this could lead to bending that triggers pulse buckling. The wavelength of bending oscillations that corresponds to this period for the example shell wall is 13 mm. This is probably a shorter wavelength than one would expect for pulse buckling dominated by early elastic response.

3.4 Concluding Remarks.

The example shell considered in this section has a wall thickness near the lower limit for which one would choose SPLAT for impulse simulation, and the 800-tap impulse is also near a lower limit, thus setting the strand spacing D near an upper limit. This combination of a thin wall and a large strand spacing is a reasonably

severe test of the tendency of SPLAT ripple to initiate pulse buckling. The results of the calculation give deformation ripples of the order of a few percent of the wall thickness, which is the same order as the imperfections that trigger pulse buckling in theoretical analyses. This would lead one to suspect that SPLAT deformation ripple might influence pulse buckling in thin-walled shells currently being tested at SRI International.

However, there are several features of the detailed forms of the deformation ripple that tend to mitigate buckle initiation:

- The shape of the deformation ripple changes in a complex way as the impulse is delivered. Thus, when structural response is taken into account, the structure stiffness will tend to resist deformation in such a complex shape.

- With the standoff-to-spacing ratio S_r taken large enough (greater than about 1.4), the deformation ripple decreases in amplitude as the impulse is delivered. (However, this decrease takes place during late times for which structural stiffness, neglected in this analysis, must be taken into account.)

- If the MDF strands are tilted with respect to the axis of the shell, to produce more nearly simultaneous impact, the resulting deformation ripple patterns change along the length of the shell, which tends to inhibit initiation of pulse buckling.

In conclusion, while the simple analysis of deformation ripple presented in this chapter and the last gives a good demonstration of the nature of the ripple, it is inconclusive as to whether the SPLAT loading interacts with structural response to give an amplitude of ripple large enough to influence the initiation of dynamic pulse buckling from natural imperfections. The amplitudes calculated in this chapter are large enough at early times to initiate buckling, but are decreasing with time at times beyond the range of validity of the analysis. In the next chapter we calculate structural response with the shell (plate) stiffness included in the analysis.

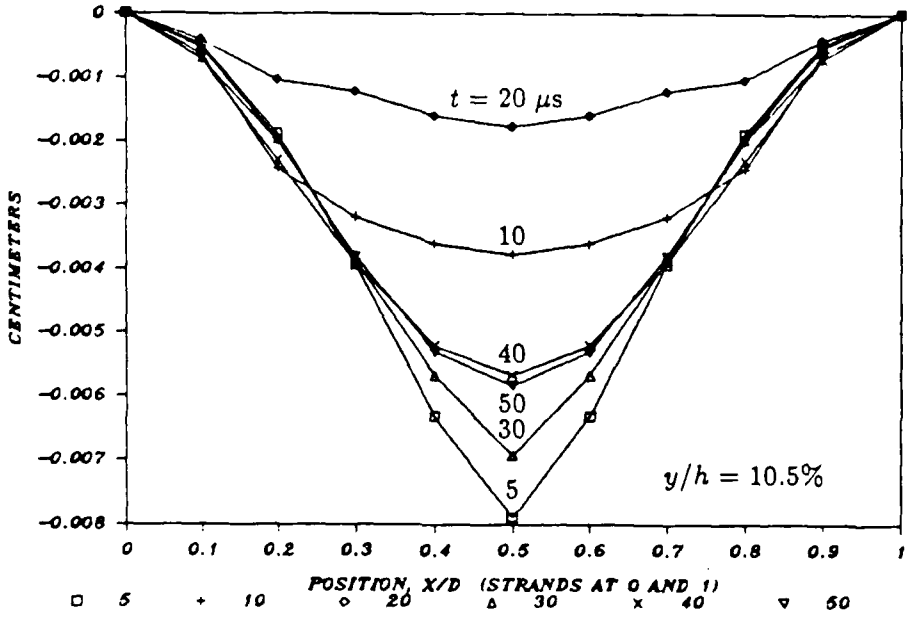

Figure 15. Strand-to-strand relative deformation shapes at a sequence of times for $S_r = 1.0$.

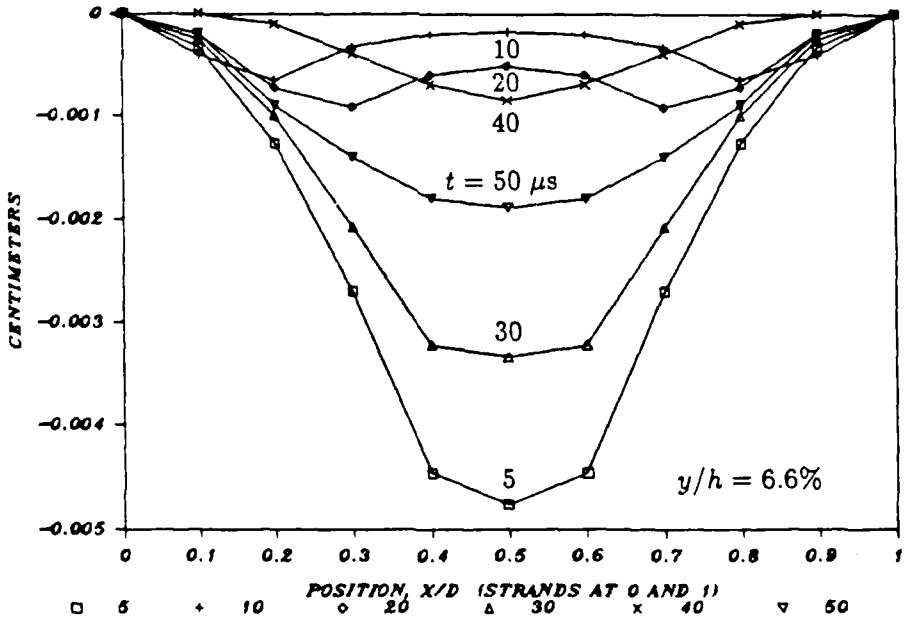

Figure 16. Strand-to-strand relative deformation shapes at a sequence of times for $S_r = 1.2$.

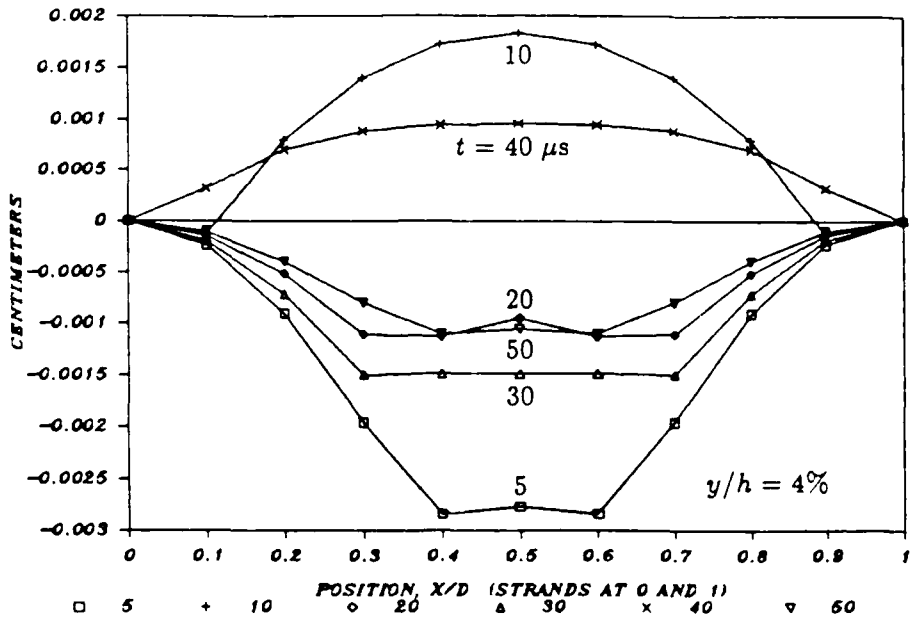

Figure 17. Strand-to-strand relative deformation shapes at a sequence of times for $S_r = 1.4$.

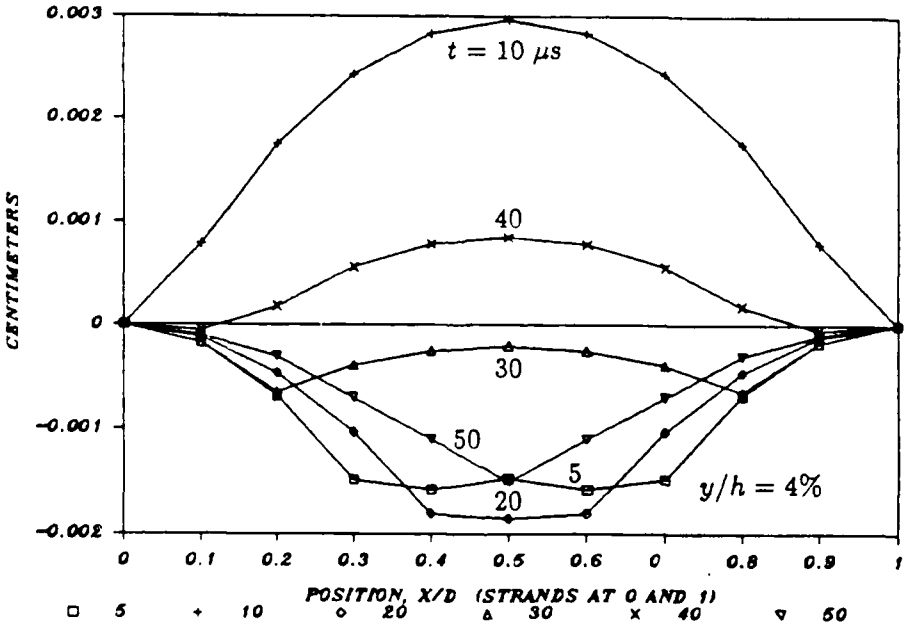

Figure 18. Strand-to-strand relative deformation shapes at a sequence of times for $S_r = 1.6$.

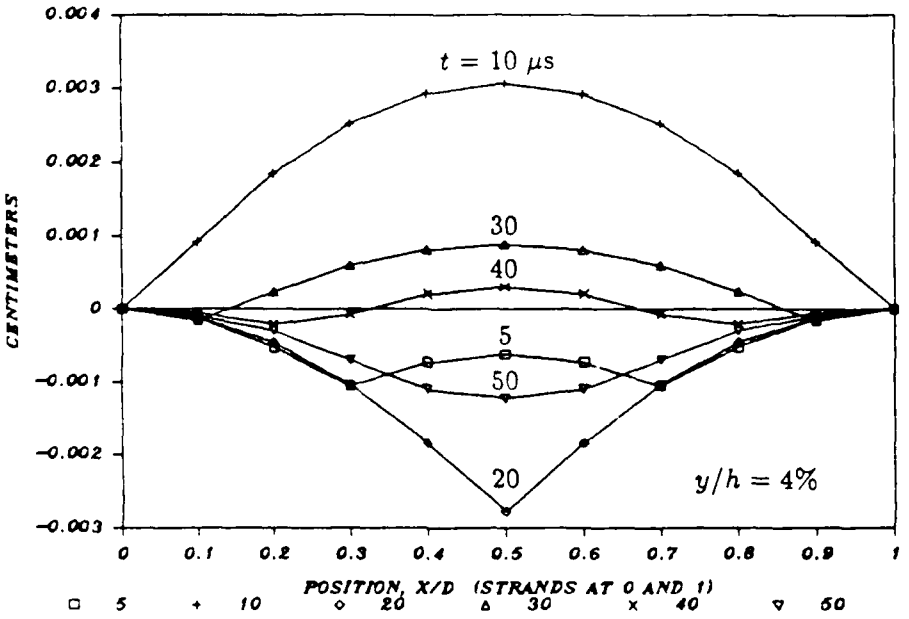

Figure 19. Strand-to-strand relative deformation shapes at a sequence of times for $S_r = 1.8$.

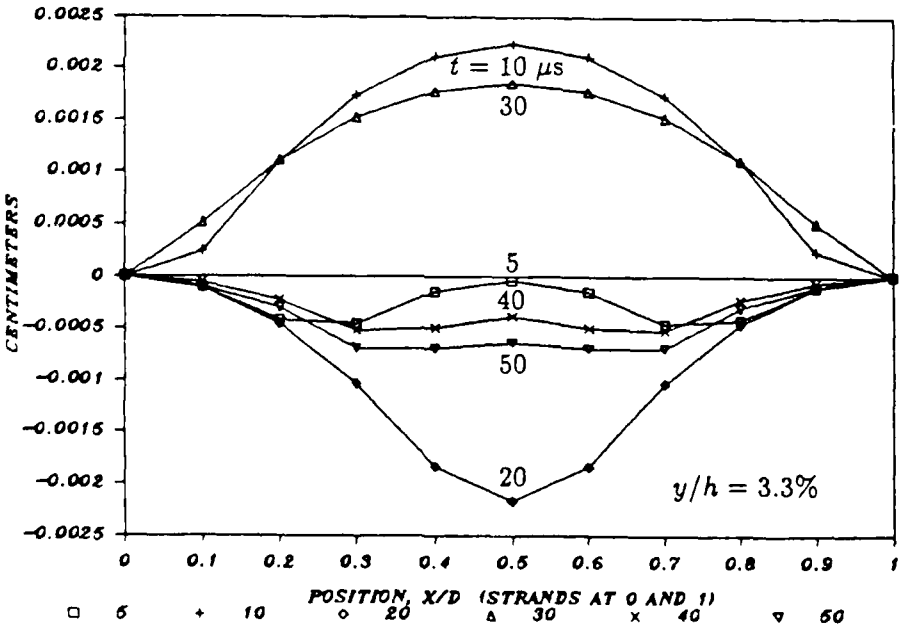

Figure 20. Strand-to-strand relative deformation shapes at a sequence of times for $S_r = 2.0$.

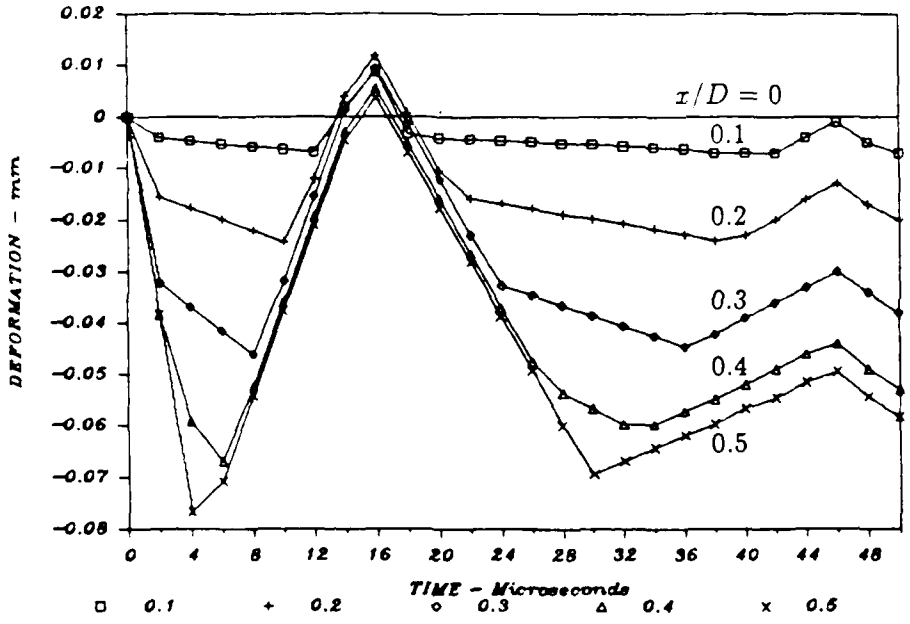

Figure 21. Relative deformation *vs.* time for $S_r = 1.0$.

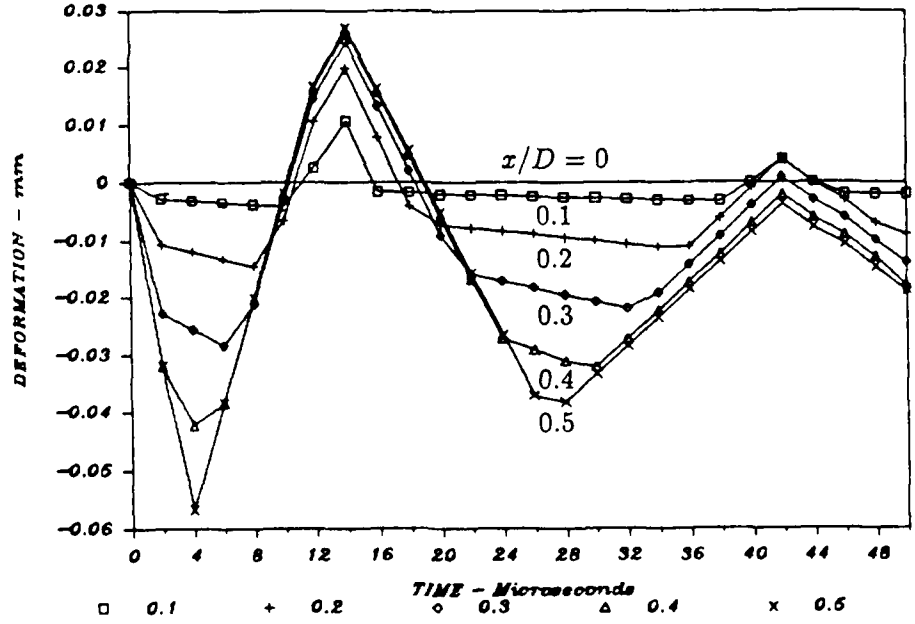

Figure 22. Relative deformation *vs.* time for $S_r = 1.2$.

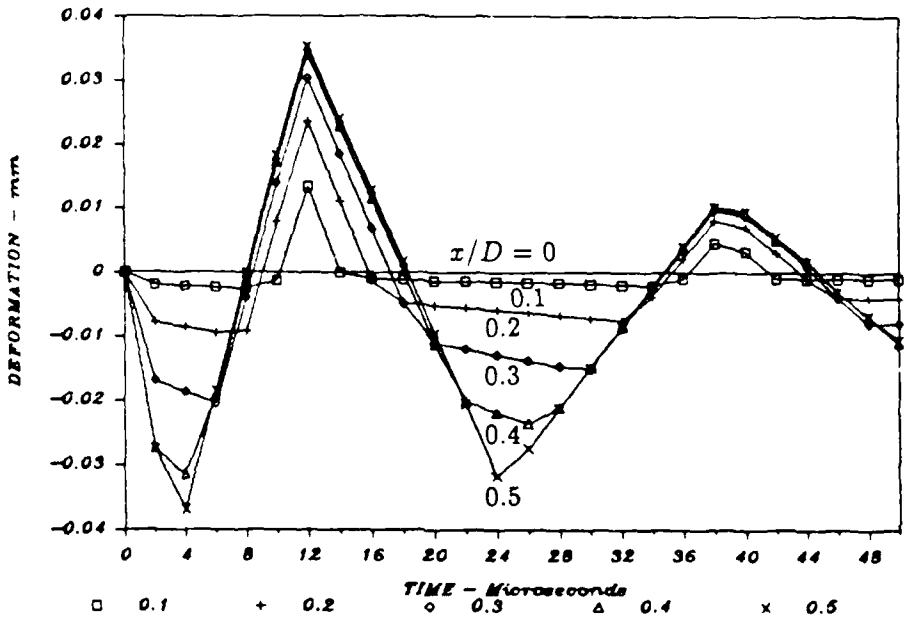

Figure 23. Relative deformation *vs.* time for $S_r = 1.4$.

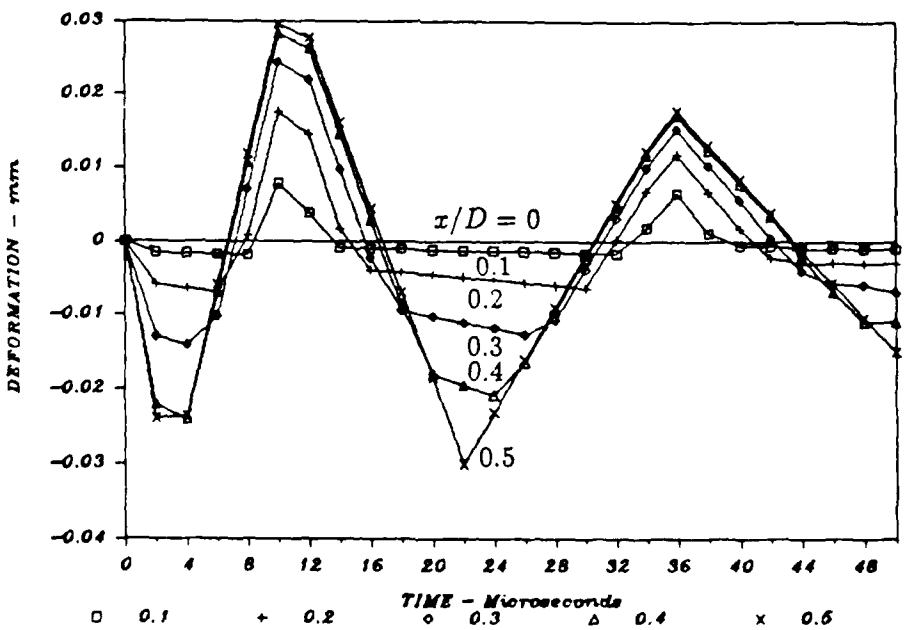

Figure 24. Relative deformation *vs.* time for $S_r = 1.6$.

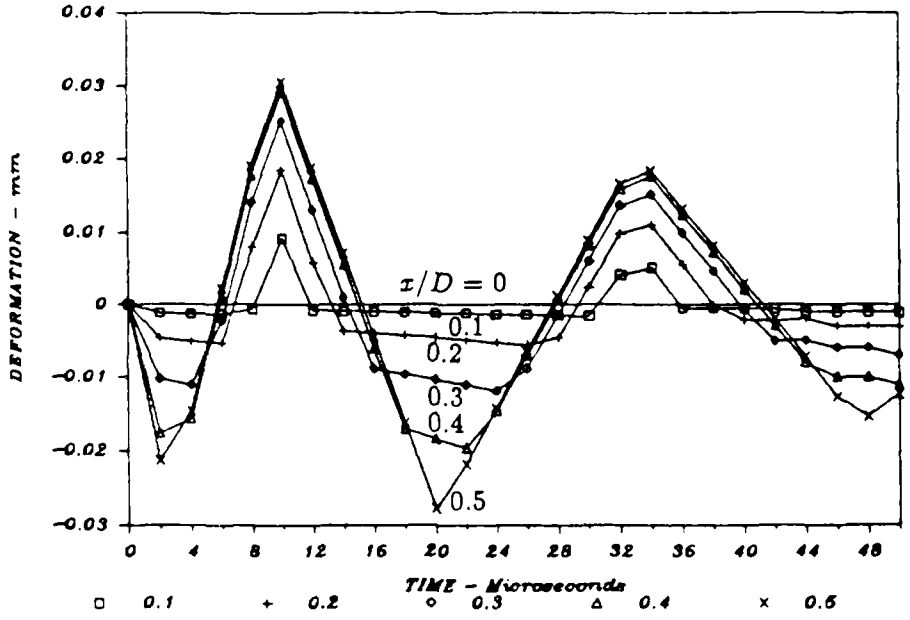

Figure 25. Relative deformation *vs.* time for $S_r = 1.8$.

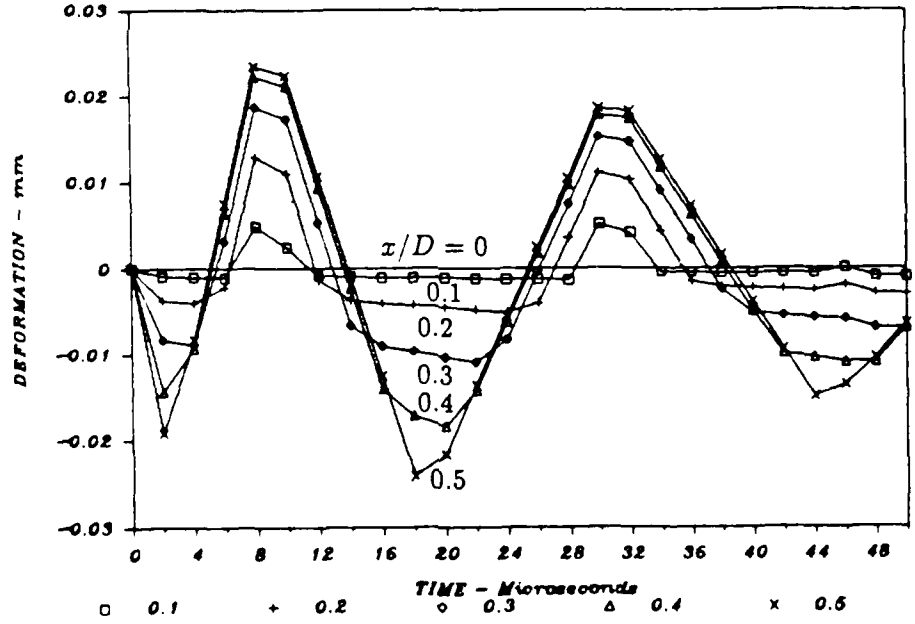

Figure 26. Relative deformation *vs.* time for $S_r = 2.0$.

SECTION 4
THEORY OF DEFORMATION RIPPLE FOR PLATES

The examples in Section 3 showed that, for standoff ratios $S_r > 1$, the deformation ripple oscillates with peak amplitudes that decrease with increasing time as impulse is delivered by strands farther away from the interval $0, D$. The maximum amplitude typically occurs just as impulse is delivered by strands once or twice removed from the interval. Then, as impulse is delivered by strands still farther from the interval, the peak amplitudes decrease. For the example shell and impulse, the times at which these later pulses arrive are larger than the quarter period of bending oscillations of the shell at the wavelength of the ripple. Thus, the early time theory in Sections 2 and 3, in which the stiffness of the shell was neglected, is not applicable during the time when the ripple amplitudes are decreasing. Since the wall thickness in the example was near the lower limit for which SPLAT is applicable, this is the typical situation.

As discussed in Section 3.1, in the example shell the period of bending oscillations at the wavelength D of the strand spacing is 98 μs and the early time theory is therefore inapplicable for times greater than about 20 μs. For larger times, bending stiffness and vibrations must be included in the response analysis. As also discussed, the period for dynamic pulse buckling to reach a maximum, when both the bending stiffness and hoop thrust are included, is about 125 μs. Hence, hoop thrust and buckling can be neglected for times less than about half this value, or about 60 μs. Thus, there is a significant time interval during which a response theory with bending, but without buckling, is applicable. This is also a typical situation; if the impulse is not delivered before significant buckling occurs, the simulation parameters are unsatisfactory.

A useful tool for analysis of deformation ripple is therefore a theory of plate response (for which there is no in-plane thrust) that includes bending vibrations but not buckling. This theory is given in the present chapter. The simpler theory in Sections 2 and 3 was presented to give a physical feel for the essentials of deformation ripple with a minimum of complications. Also, without the further complication of target vibrations, there are fewer parameters and the results in Section 3, while given for a specific case, are actually quite general within the time limitations just discussed. When buckling is included in addition to bending vibrations, the number of parameters becomes so large that it is difficult to generalize results from the theory. This is particularly true for elastic-plastic flow buckling, which occurs in all but the thinnest shells. For this analysis, the finite element method is most appropriate, as given in Section 5.

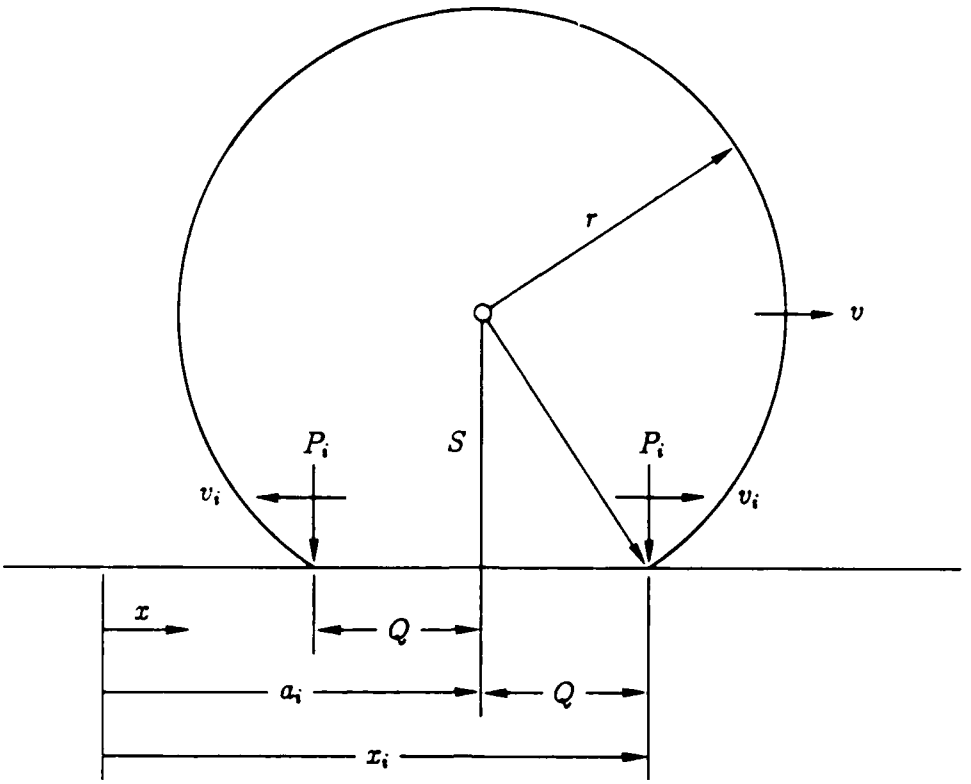

Figure 27. Symmetric running loads from i^{th} strand.

4.1 Equations of Motion.

Analysis of plate response to SPLAT loading is done with finite Fourier transforms on the central interval $x = 0, D$ between adjacent strands of the array in Figure 1. The loading of lead impact from the i^{th} MDF strand is idealized as two symmetric concentrated forces of magnitude P_i traveling at velocites $\pm v_i$ as shown Figure 27. Both the magnitude P_i and velocity v_i vary with time as the arc of lead spray expands (see Figure 2). The equations of motion of the plate are those of a rectangular beam, since we consider that the plate is infinite in extent in the direction into the paper. The contribution to the lateral motion $y(x,t)$ from, say, the forward running load from the i^{th} strand is given by the equation of motion

$$y_{i,zzzz} + \frac{\rho A}{EI} y_{i,tt} = \frac{P_i}{EI} \cdot \delta(x - x_i) \tag{23}$$

where ρ is material density, A is section area, E is Young's modulus, I is the moment of inertia of the section, and δ is the Dirac delta function. The position coordinate is x, as shown in Figure 1, and x_i is the position of P_i. The $,x$ and $,t$ subscripts on y_i denote partial differentiation with respect to x and t, respectively.

The boundary conditions at the ends of the interval $0, D$, by symmetry of the

beam shape in every interval D between strands in a uniform array, are those of zero slope and zero shear force:

$$y_{,x}(0) = y_{,xxx}(0) = y_{,x}(D) = y_{,xxx}(D) = 0 \tag{24}$$

The magnitude of the force P_i is expressed in terms of the impulse delivered by lead impact as the spray expands. Thus, as P_i crosses an elemental length of plate dx_i, the impulse delivered in time dt is equal to the momentum imparted to this elemental length.

$$P_i\, dt = \rho A\, dx_i \cdot V_i = \rho A V_i \cdot dx_i = I_i b\, dx_i \tag{25}$$

or

$$P_i = I_i b \frac{dx}{dt} = I_i b\, x_{i,t} \tag{26}$$

where V_i is the velocity imparted to the element at running load location x_i by the i^{th} strand, I_i is the corresponding impulse intensity per unit area as derived in Section 2, and b is the width of the plate in the direction into the paper ($A = bh$). An expression for the velocity $v_i = x_{i,t}$ of the running load is found by solving Eq. (8) for x_i and then differentiating with respect to time. With $r = S + vt$ from Eq. (15) (we drop the subscript i because for the uniform array under consideration the instantaneous expansion radii of all the lead sprays are identical) Eq. (8) becomes

$$(S + vt)^2 = (x_i - a_i)^2 + S^2 \tag{27}$$

The subscript i has been added to x because we are now considering motion of the entire plate from the i^{th} strand rather than making the simple calculations of impulse and motion at location x as was done in Section 2. Solving for x_i gives

$$x_i = [2Svt + v^2t^2]^{1/2} + a_i \tag{28}$$

Differentiation and some manipulation gives

$$x_{i,t} = \frac{vr}{[2Svt + v^2t^2]^{1/2}} = \frac{vr}{x_i - a_i} \tag{29}$$

Note that the second expression for velocity can be written directly from the geometry in Figure 2. However, the first expression is the one to be used in calculations. For convenience, we therefore define

$$Q = [2Svt + v^2t^2]^{1/2} \tag{30}$$

With impulse I_i from Eq. (9) and $x_{i,t}$ from Eq. (29), Eq. (26) becomes

$$P_i = \frac{bmvS^2}{2\pi r_i^3} \cdot \frac{vr_i}{Q} = \frac{bmv^2S^2}{2\pi Q r_i^2} \tag{31}$$

It will be convenient later to again express the constants in this expression in terms of the uniform-impulse velocity V imparted to the plate by the strand array. Thus, we use Eq. (21) to obtain

$$P_i(t) = \frac{\rho A V D v S^2}{2Q(t) r_i^2(t)} \tag{32}$$

It is also convenient to express Eq. (28) in terms of Q.

$$x_i(t) = a_i + Q(t) \tag{33}$$

This is the load location for the forward running spray from each strand. From Figure 2 it is immediately apparent that the loads from the backward running sprays have the same magnitude as for the forward sprays and are located at

$$x_i(t) = a_i - Q(t) \tag{34}$$

4.2 Solution by Finite Fourier Transforms.

The finite Fourier cosine transform is defined by (see, e.g., Reference 3, p. 272):

$$\mathcal{Y}(n,t) = \int_0^D y(x,t) \cos \frac{n\pi x}{D}\, dx \equiv C\{y\} \tag{35}$$

The inversion formula is

$$y(x,t) = \frac{1}{D}\mathcal{Y}(0,t) + \frac{2}{D}\sum_{n=1}^{\infty} \mathcal{Y}(n,t) \cos \frac{n\pi x}{D} \equiv C^{-1}\{\mathcal{Y}\} \tag{36}$$

The operational properties to the order needed here are:

$$C\{y_{,xx}\} = -\frac{n^2\pi^2}{D^2}\mathcal{Y} - y_{,x}(0) + (-1)^n y_{,x}(D) \tag{37}$$

$$\begin{aligned} C\{y_{,xxxx}\} &= \frac{n^4\pi^4}{D^4}\mathcal{Y} + \frac{n^2\pi^2}{D^2}\left[y_{,x}(0) - (-1)^n y_{,x}(D)\right] \\ &\quad - \left[y_{,xxx}(0) - (-1)^n y_{,xxx}(D)\right] \end{aligned} \tag{38}$$

These properties are appropriate for boundary conditions (24), which is why Fourier cosine transforms were chosen for the solution. With these definitions, differential equation (23) with boundary conditions (24) becomes

$$\frac{n^4\pi^4}{D^4}\mathcal{Y}_i + \frac{\rho A}{EI}\mathcal{Y}_{i,tt} = \frac{P_i(t)}{EI} \cos \frac{n\pi x_i(t)}{D} \tag{39}$$

or, upon rearrangement,

$$\mathcal{Y}_{i,tt} + \frac{n^4\pi^4}{D^4}\frac{EI}{\rho A}\mathcal{Y}_i = \frac{P_i}{\rho A}\cos\frac{n\pi x_i(t)}{D} \tag{40}$$

From Eq. (40), the circular frequency of vibration of the n^{th} mode of vibration of the beam segment in the interval $0, D$ is given by

$$\omega_n^2 = \frac{n^4\pi^4}{D^4}\frac{EI}{\rho A} = \frac{n^4\pi^4 c^2 h^2}{12D^4} \tag{41}$$

where h is the depth of the beam (thickness of the plate) and c is the axial wave velocity in the beam (membrane wave velocity in the plate).

Modal equation (40) for the finite Fourier transform is solved by the Duhamel integral, with general solution

$$\begin{aligned}\mathcal{Y}_i(n,t) &= C_{in}\sin\omega_n t + D_{in}\cos\omega_n t + \\ &\quad \frac{1}{\rho A\omega_n}\int_0^t P_i(\tau)\cos\frac{n\pi x_i(\tau)}{D}\cdot\sin\omega_n(t-\tau)\,d\tau\end{aligned} \tag{42}$$

Substitution of this solution into the transformed initial conditions

$$\mathcal{Y}(n,0) = \mathcal{Y}_{,t}(n,0) = 0 \tag{43}$$

gives $C_{in} = D_{in} = 0$. The contribution to the finite Fourier transform (motion in the n^{th} mode) from the i^{th} strand is then simply

$$\mathcal{Y}_i(n,t) = \frac{1}{\rho A\omega_n}\int_0^t P_i(\tau)\cos\frac{n\pi x_i(\tau)}{D}\cdot\sin\omega_n(t-\tau)\;d\tau \tag{44}$$

To evaluate the integral, we expand

$$\sin\omega_n(t-\tau) = \sin\omega_n t\cos\omega_n\tau - \cos\omega_n t\sin\omega_n\tau \tag{45}$$

Then

$$\mathcal{Y}_i(n,t) = A_{in}(t)\cos\omega_n t + B_{in}(t)\sin\omega_n t \tag{46}$$

where

$$A_{in}(t) = \frac{-1}{\rho A\omega_n}\int_0^t P_i(\tau)\cos\frac{n\pi x_i(\tau)}{D}\cdot\sin\omega_n\tau\;d\tau \tag{47}$$

$$B_{in}(t) = \frac{1}{\rho A\omega_n}\int_0^t P_i(\tau)\cos\frac{n\pi x_i(\tau)}{D}\cdot\cos\omega_n\tau\;d\tau \tag{48}$$

With $\mathcal{Y}_i(n,t)$ found by using Eqs. (46–48), the motion $y_i(x,t)$ is recovered with inversion formula (36). The final solution is a double summation over i and n. The

integrals in Eqs. (47) and (48) are found by numerical integration using $P_i(t)$ and $x_i(t)$ from Eqs. 32 and 33, respectively.

By inspection of Figure 1, it is apparent that motion in the interval $0, D$ is symmetric about the central location $x = D/2$, as is motion in every interval between strands in an infinite array. Similarly, motion is symmetric about the strand location points in the infinite array. This latter symmetry was used to define the boundary conditions in Eq. 24 and hence dictated the use of finite Fourier cosine transforms for solution. The symmetry about the strand interval midpoints results in only even modes of the cosine shape functions being excited.

Thus, when both the forward and backward running loads are included in the calculations, the odd mode motion excited by forward running loads is cancelled by the odd mode motion excited by backward running loads. Similarly, the even mode motion from backward running loads is identical with that from the forward running loads. Thus, motion is calculated with only even modes and forward running loads, with the amplitude doubled to account for the backward running loads.

4.3 Example Ripple Deformations.

The above equations for deformation ripple of plates were integrated numerically by Simpson's rule with the Pascal program given in Appendix A. The singularity at $t = 0$, when the running load amplitude and velocity from the strand at $x = 0$ are infinite, was treated by stepping through the first time increment Δt in 10 steps. Also, interactive input to the program calculates the maximum allowable time increment such that during Δt the running load from the strand at $x = 0$ moves only a specified fraction of the wavelength of the highest mode to be included in the Fourier transform.

Example deformation shapes and amplitudes are given in Figures 28 through 39. Shapes are given in Figure 28 at selected times for 800 taps applied to a 0.762-mm-thick plate of aluminum with a strand spacing $D = 26$ mm and a standoff ratio $S_r = 1$. At 5 μs the shape is approximately a complete cosine wave ($n = 2$) with a peak amplitude of 0.036 mm (4.7% of the plate thickness) occurring between strands. At 15 μs the phase of this deformation is reversed and the $n = 8$ harmonic has appreciable amplitude. Further shapes for this example are given in Figure 29.

The times selected for display here are those at which the amplitudes of motion are near local maxima. Typically, the maxima are associated with relative deformation between points directly under strands ($x = 0$) and midway between strands ($x = D/2$). Thus, 'peak-to-peak' deformation between these points is plotted in Figure 30. Note that the times in the plots of Figures 28 and 29 are near times at which the peak-to-peak deformation has local maxima. Observe also that the values of the larger maxima are sustained throughout the 50 μs for which plate theory can be used to approximate shell response (i.e., before significant buckling for the

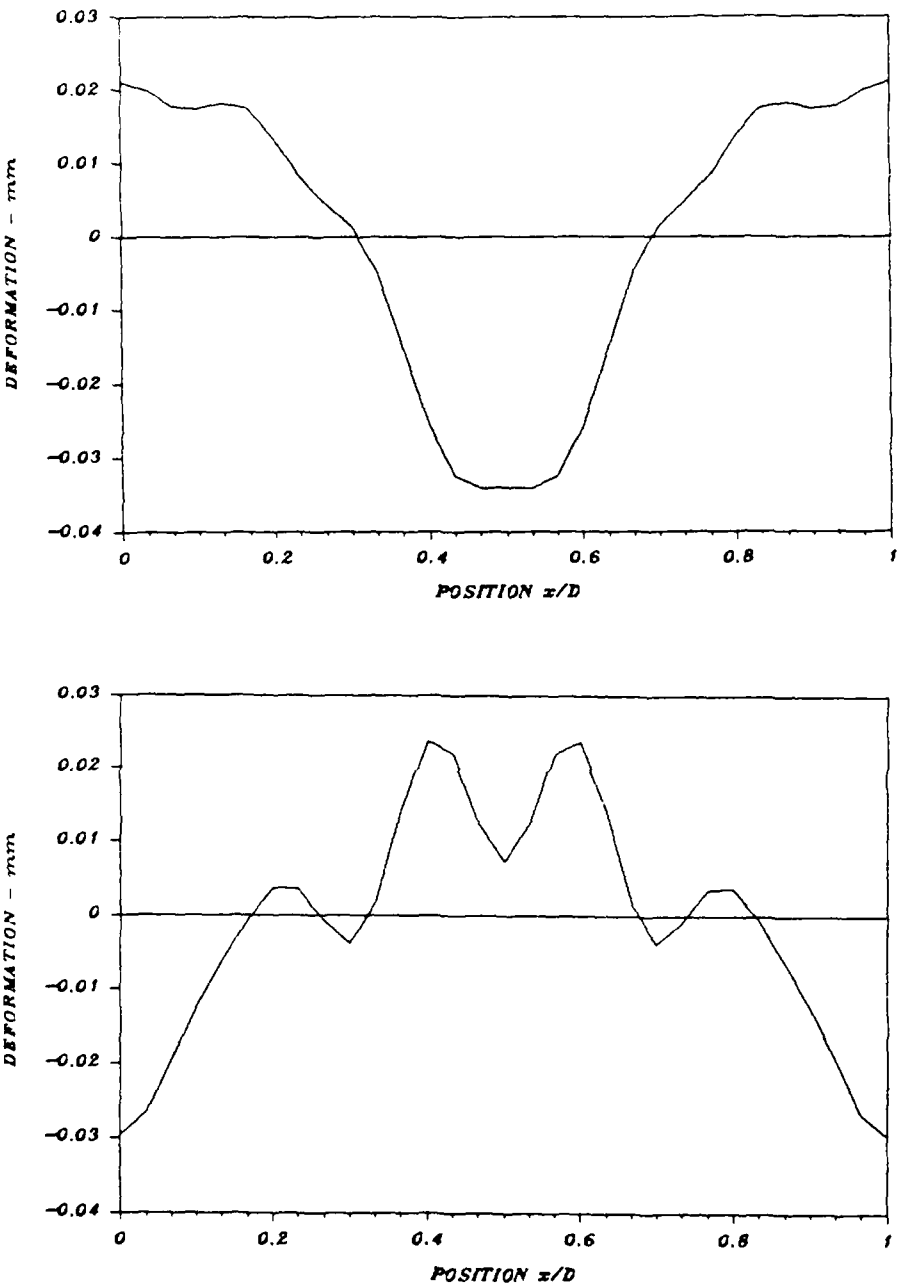

Figure 28. Plate deformation shapes at $t = 5$ and 15 μs, with 800 taps, $h = 0.762$ mm, $D = 26$ mm, $S_r = 1$.

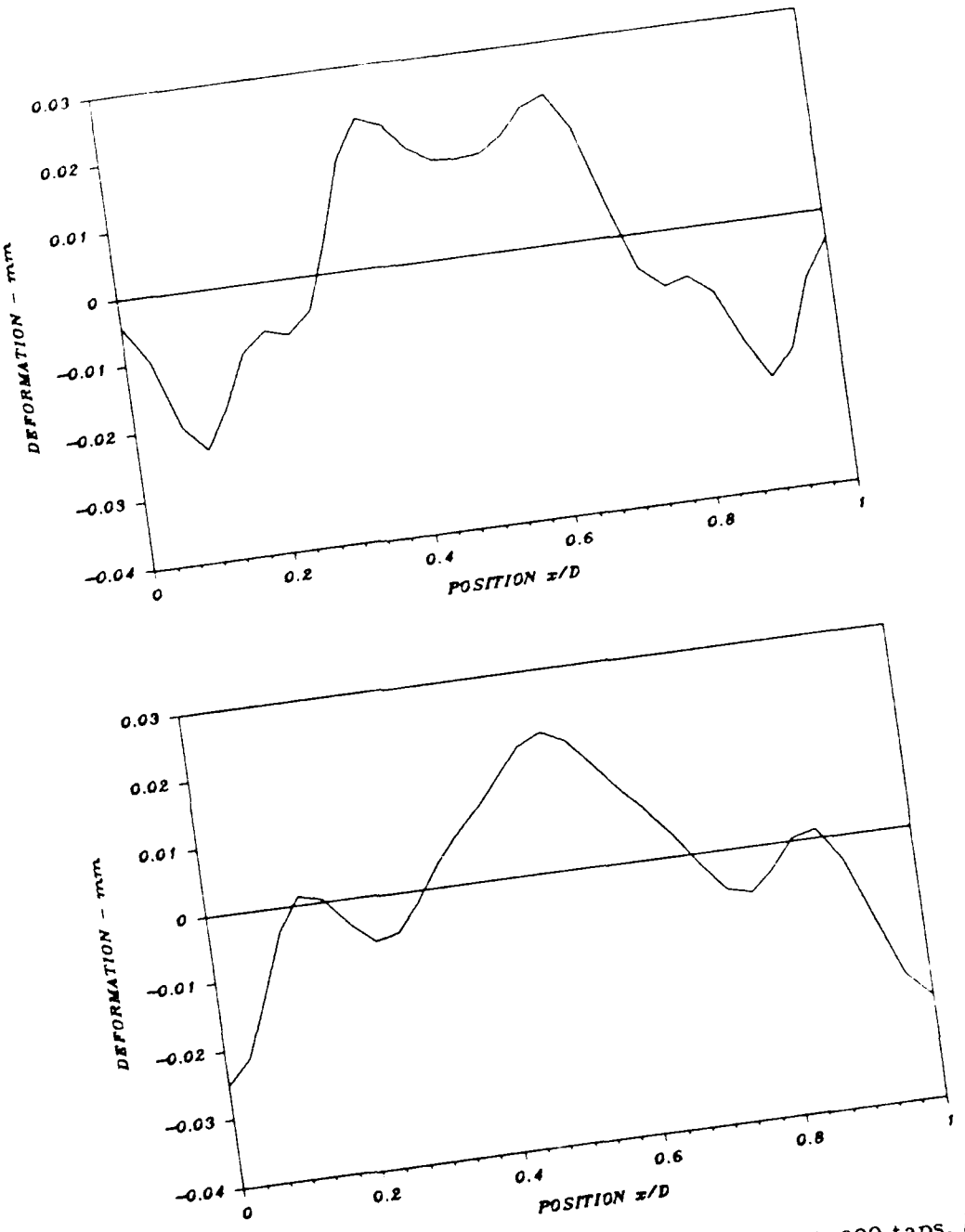

Figure 29. Plate deformation shapes at $t = 19$ and 44 μs, with 800 taps, $h = 0.762$ mm, $D = 26$ mm, $S_r = 1$.

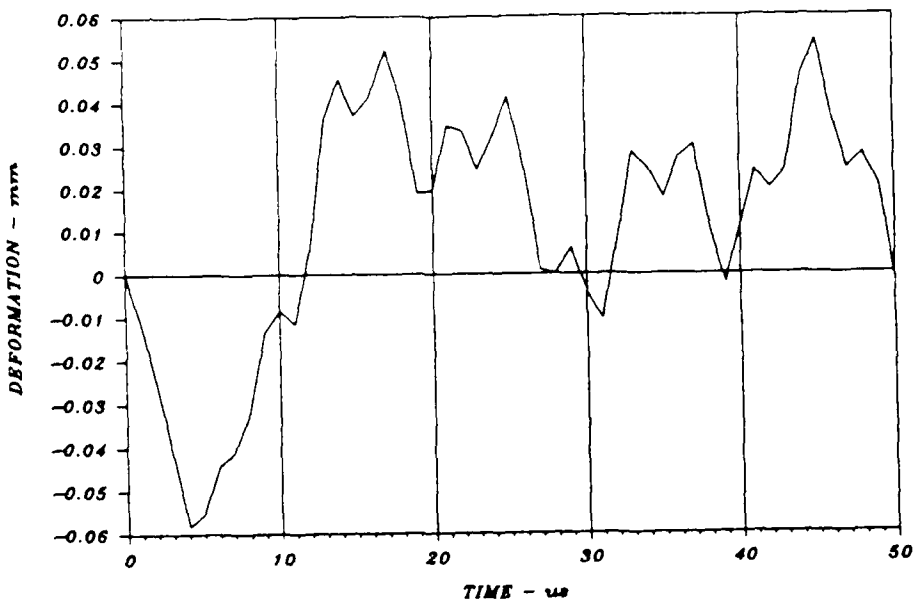

Figure 30. Peak-to-peak deformation *vs.* time, with 800 taps, $h = 0.762$ mm, $D = 26$ mm, $S_r = 1$.

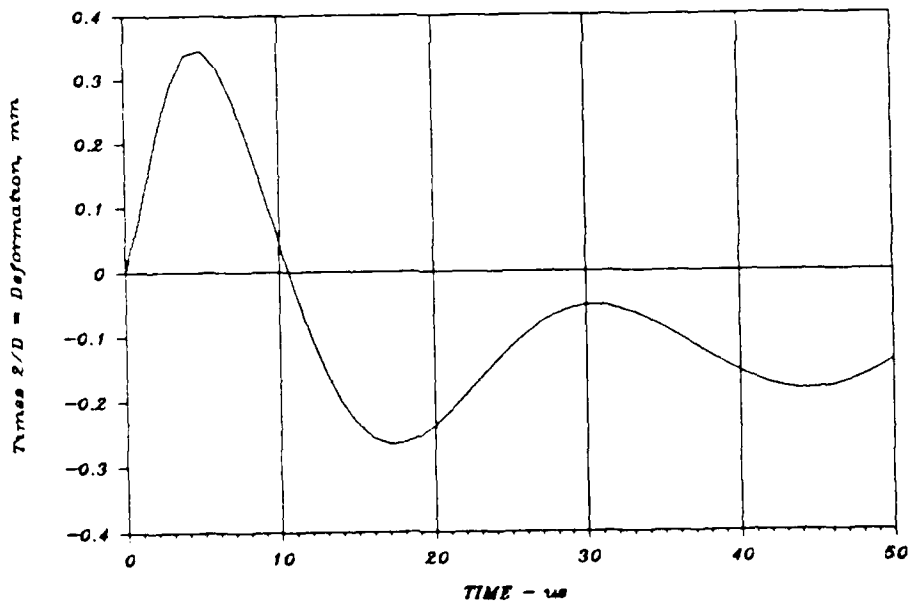

Figure 31. Fourier cosine transform for $n = 2$, with 800 taps, $h = 0.762$ mm, $D = 26$ mm, $S_r = 1$.

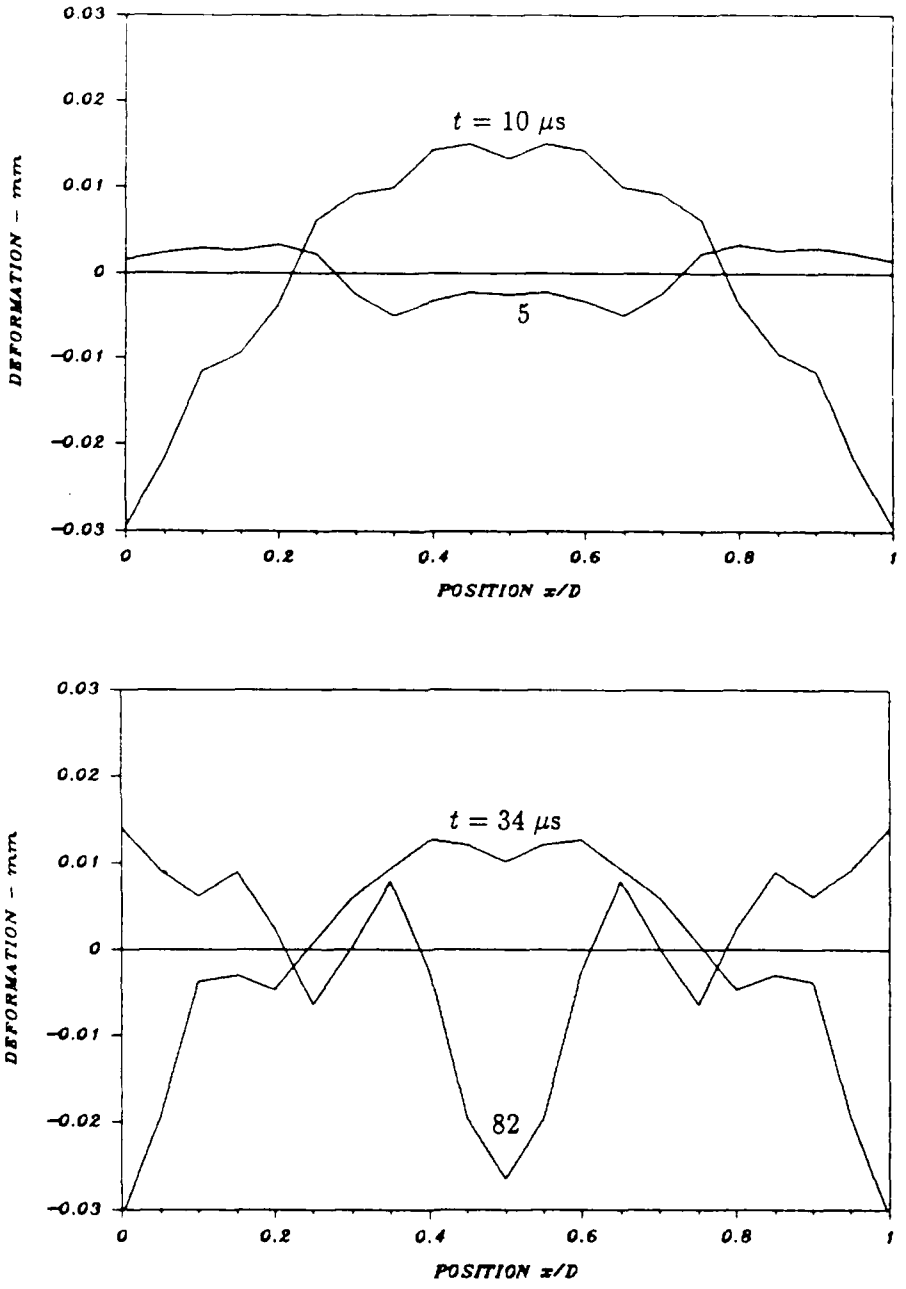

Figure 32. Plate deformation shapes at $t = 5$, 10, 34, and 82 μs, with 800 taps, $h = 0.762$ mm, $D = 26$ mm, $S_r = 1.6$.

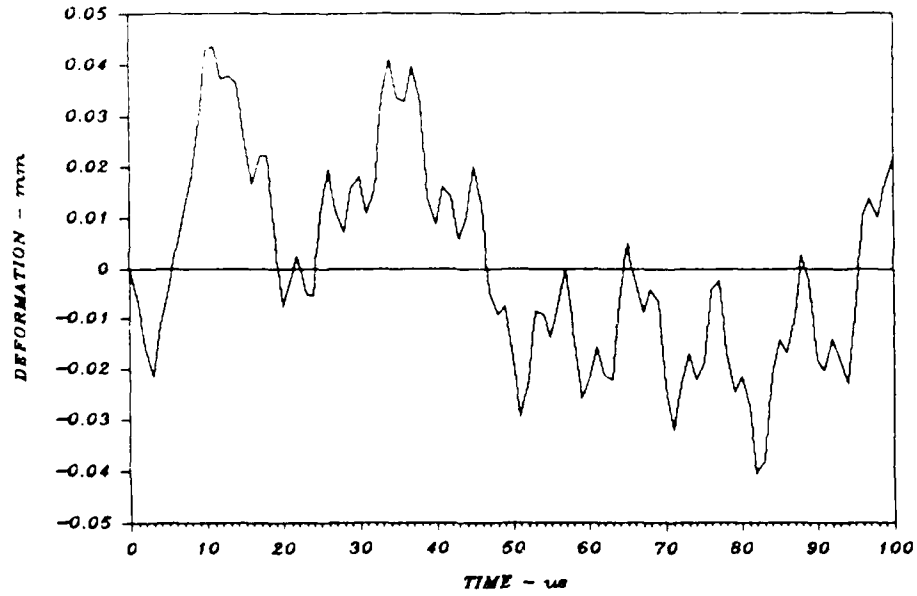

Figure 33. Peak-to-peak deformation *vs.* time, with 800 taps, $h = 0.762$ mm, $D = 26$ mm, $S_r = 1.6$.

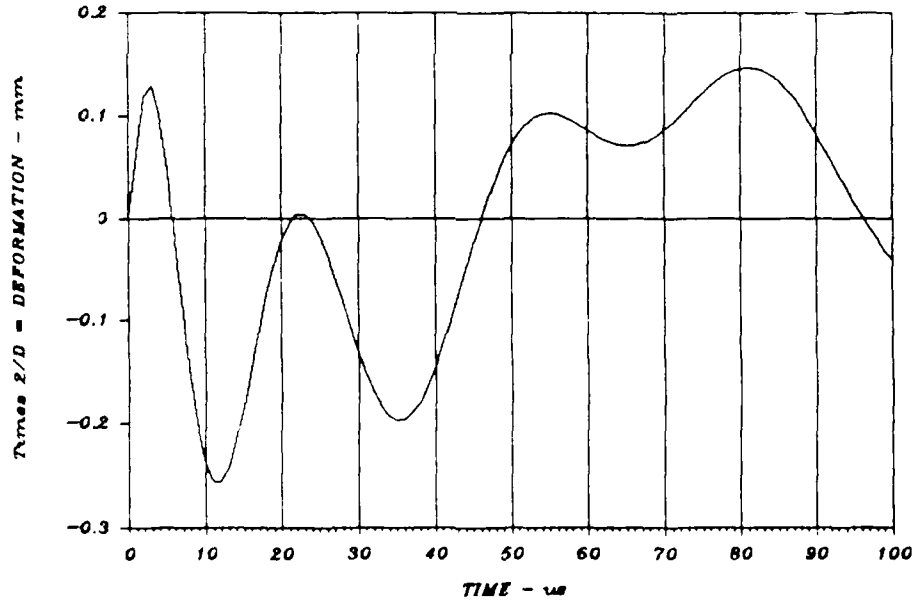

Figure 34. Fourier cosine transform for $n = 2$, with 800 taps, $h = 0.762$ mm, $D = 26$ mm, $S_r = 1.6$.

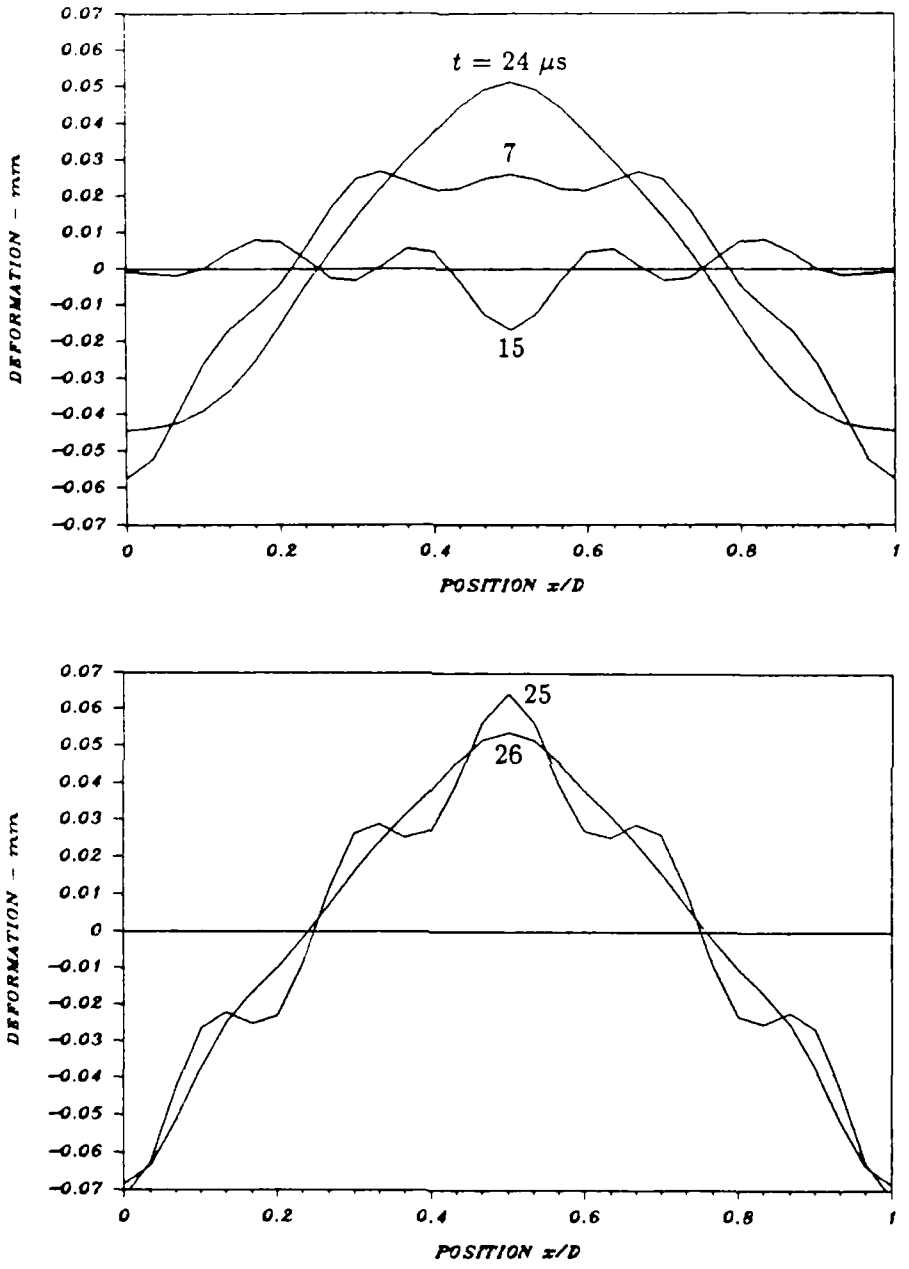

Figure 35. Plate deformation shapes at t = 7, 15, 24, 25, 25 μs, with 2100 taps, h = 0.635 mm, D = 26 mm, S_r = 2.4.

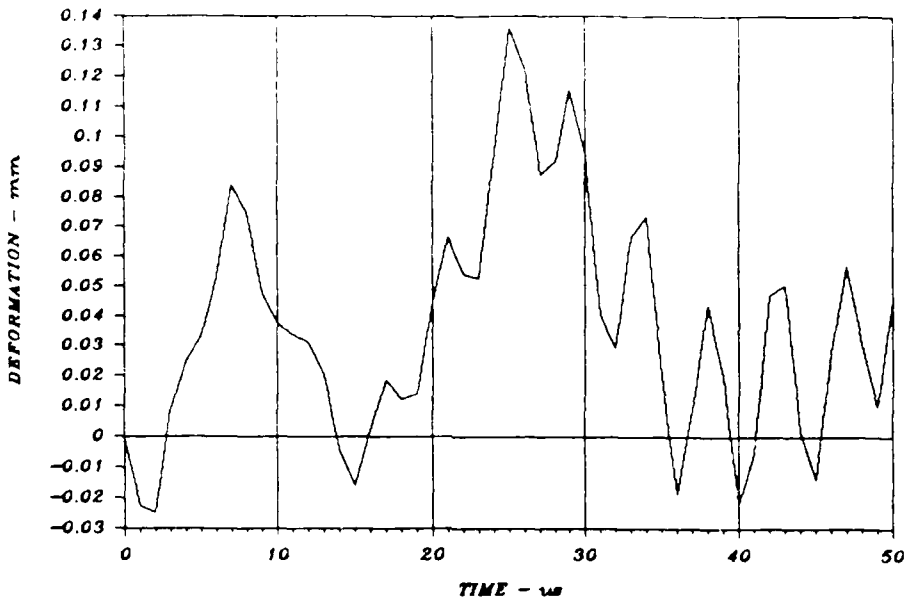

Figure 36. Peak-to-peak deformation *vs.* time, with 2100 taps, $h = 0.635$ mm, $D = 26$ mm, $S_r = 2.4$.

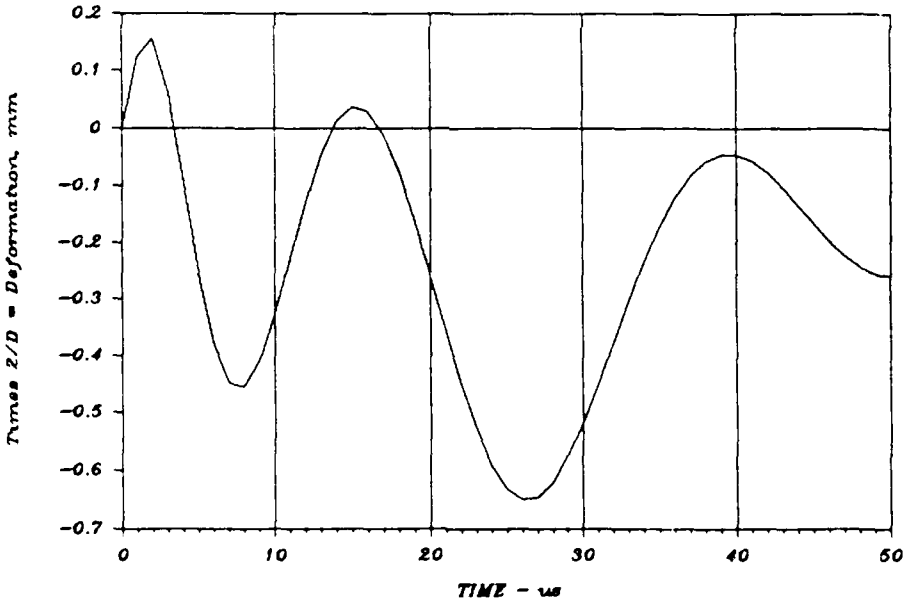

Figure 37. Fourier cosine transform for $n = 2$, with 2100 taps, $h = 0.635$ mm, $D = 26$ mm, $S_r = 2.4$.

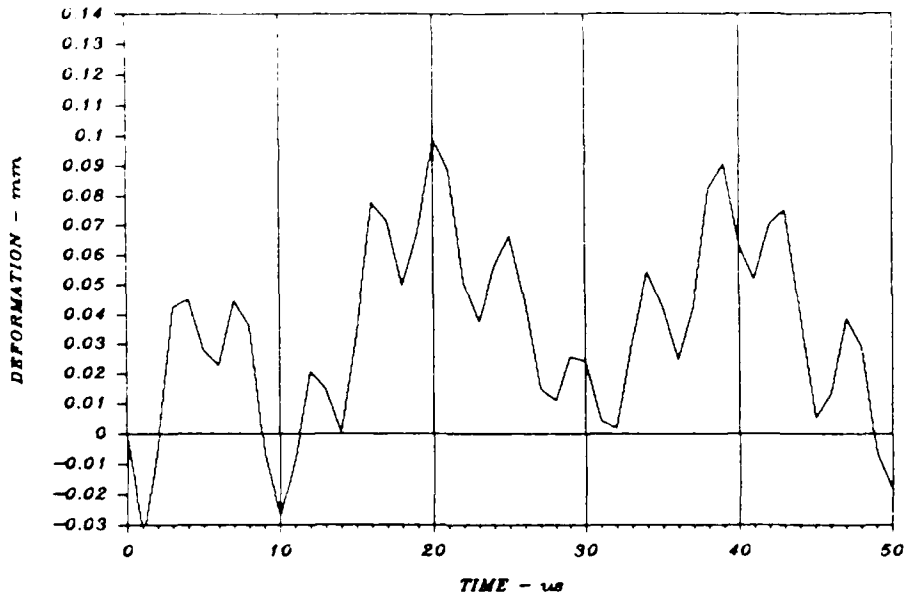

Figure 38. Peak-to-peak deformation *vs.* time, with 2100 taps, $h = 0.635$ mm, $D = 26$ mm, $S_r = 3.4$.

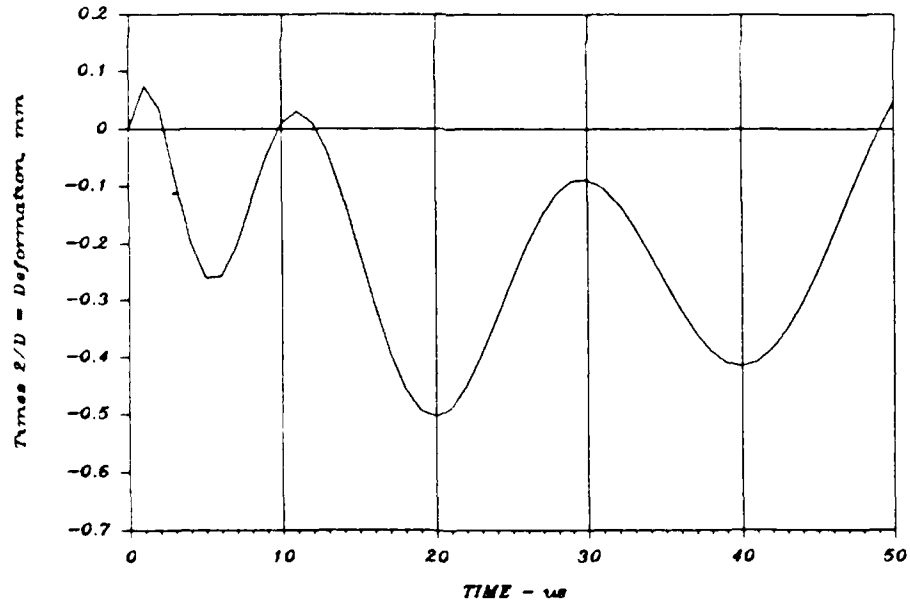

Figure 39. Fourier cosine transform for $n = 2$, with 2100 taps, $h = 0.635$ mm, $D = 26$ mm, $S_r = 3.4$.

shell dimensions in the previous chapters). The maximum peak-to-peak amplitude is 0.058 mm, which corresponds to a one-sided peak amplitude of 3.8% of the plate thickness.

The $n = 2$ component of the Fourier cosine transform for this example is plotted in Figure 31. The important observation is that the dominant peaks of the total peak-to-peak deformation in Figure 29 nearly coincide with the peaks of the $n = 2$ component of the Fourier cosine transform. Thus, as one might anticipate, while there are significant vibrations in the higher harmonics, the maximum deformations are dominated by the fundamental mode (the lowest even harmonic).

Figures 32 through 34 give similar results for the same plate and loading parameters but with standoff ratio $S_r = 1.6$. The details differ but the overall features of response are similar. The maximum peak-to-peak amplitude, from Figure 33, is 0.043 mm, which corresponds to a one-sided peak amplitude of 2.8% of the plate thickness. Both the peak-to-peak amplitude and $n = 2$ Fourier transform plots show that, unlike the deformation ripple calculated in Sections 2 and 3 with plate bending stiffness neglected, the plate vibration modes tend to sustain this amplidude at later times.

Similar results are given in Figures 35 through 37 for $S_r = 2.4$, and in Figures 38 and 39 for $S_r = 3.4$. In these examples, the plate thickness is 0.635 mm and the impulse has been increased to 2100 taps by using 5 gr/ft MDF in place of 2 gr/ft with the same spacing $D = 26$ mm. Again, while the amplitudes tend to decrease with increasing S_r, the decrease is not great. Also, with these larger values of S_r the largest amplitudes occur later in time, after some oscillation of the plate. Once again, the largest peaks are dominated by motion in the $n = 2$ mode, as can be seen by comparing the peak-to-peak deformation plots with the Fourier cosine transform plots for $n = 2$.

4.4 Concluding Remarks.

Deformation ripple response with plate stiffness and bending vibrations included in the analysis show that the amplitudes of ripple motion are similar to those calculated in Sections 2 and 3 with bending stiffness neglected. An important new result is that the plate vibrations tend to sustain the deformation ripple out to late times. Thus, the early deformation ripple set in motion by differential arrival times of the lead sprays continues as plate vibration rather than being gradually reduced by lead spray from farther strands, as was the case in the calculations with bending stiffness neglected.

Because of the complexity of the motion and the many plate and SPLAT parameters, it is difficult to draw general conclusions concerning the absolute magnitudes of the plate ripple deformations and the details of the motion. To aid in the design of specific SPLAT arrays, an interactive graphic display program was written as

an adjunct to the ripple calculation program in Appendix A. This program, listed in Appendix B, takes output files from the program in Appendix A and displays ripple deformation plots as in the examples in the previous section, but at higher time and spatial resolution. The display program allows one to display deformation shapes at any sequence of times at any desired amplification, and repeat the display as often as desired. The plots appear on the screen quickly enough to give a slow-motion movie effect. The program was written for an IBM PC with both a graphics and monochrome text display, but can be easily modified to run with other display arrangements.

SECTION 5
FINITE ELEMENT CALCULATIONS OF RIPPLE AND BUCKLING

The primary concern caused by the small deformation ripples calculated in the previous sections is that they may initiate dynamic pulse buckling that differs from pulse buckling of shells with natural imperfections. In this section we present results of finite element calculations made with DYNA2D for plate ripple (without buckling, as in Section 4) and for shell buckling with some of the same loads and wall thicknesses as in Section 4.

Figure 40 gives plate deformation shapes for the same set of parameters used in calculating the shapes in Figure 32 by the Fourier cosine transform method. As in Section 4, the section of plate is that between two MDF strands in an infinite array. In Figure 40, dimensions normal to the plate, including the plate thickness, are amplified by a factor of 50 compared with the width dimension between strands. Deformation amplitudes can be deduced by using the plate thickness in the figure as a basis of reference. The agreement between the shapes and amplitudes from the two calculation methods is quite good. The shape at 15 μs shows appreciable vibrations in higher harmonics, just as observed in the Fourier cosine transform calculations. Similar comparisons were made for a more complete sequence of times for both $S_r = 1.0$ and $S_r = 1.6$ with similar agreement.

Figure 41 gives a plot of peak-to-peak deformation versus time from the calculation used to prepare Figure 40. Comparison of this figure with Figure 33 again confirms that the two calculation methods give essentially the same results. A comparison of peak-to-peak deformations for $S_r = 1.0$ is made between Figures 42 and 30. Again, the agreement is quite good.

Results from a DYNA2D buckling calculation (with cylindrical shell geometry rather than plate geometry) are given in Figure 43 for the same loading and wall thickness parameters as in the Fourier cosine transform calculation used to prepare Figures 35, 36 and 37. An interesting feature of the buckling results is that the shell initially buckles into the $n = 6$ harmonic (3 full waves in the MDF strand spacing interval). However, throughout the motion the shell also buckles into the $n = 2$ harmonic and by $t = 100$ μs the dominant motion has its largest bending at locations directly under and midway between strands. But even at this time higher harmonics give more nearly straight sections between these bends than for motion entirely in the $n = 2$ harmonic. Nevertheless, the dominant plastic hinges (the DYNA2D calculations were made with an elastic-plastic strain hardening material model) form at a wavelength corresponding to $n = 2$.

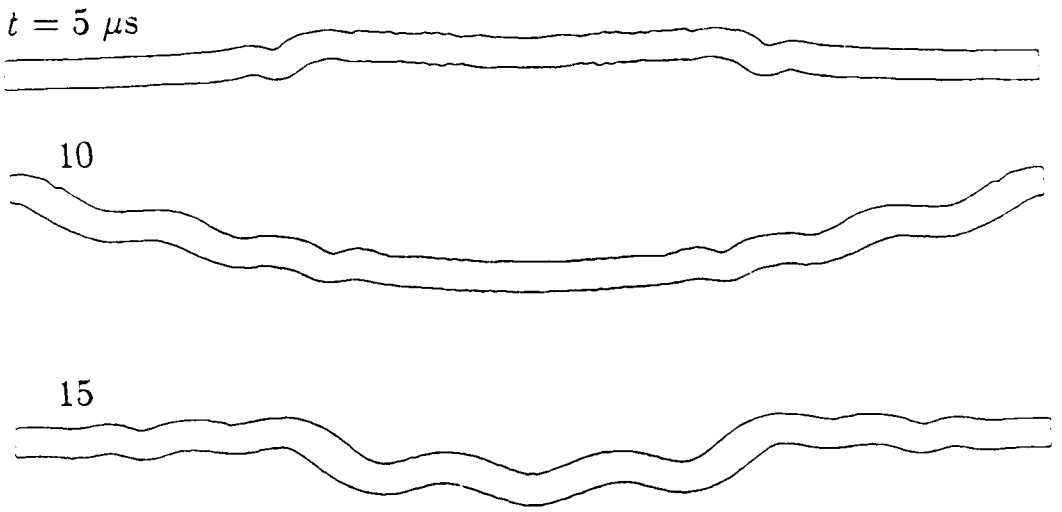

Figure 40. Plate deformation shapes from DYNA2D at t = 5, 10 and 15 μs, with 800 taps, h = 0.762 mm, D = 26 mm, S_r = 1.6.

We conclude that deformation ripple from SPLAT loading is large enough to initiate dynamic pulse buckling in thin cylindrical shells. Measurements of natural shell imperfections are needed (either made directly or by interpretations of pulse buckling experiments) in order to determine whether these deformation ripples, which are a few percent of the wall thickness in the absence of buckling, can dominate over natural imperfections. Also, as mentioned in the concluding remarks of Section 3, when the MDF strands are tilted relative to the shell wall generator the ripple deformation is not uniform along the length of the shell as in these simple example calculations. This nonuniformity introduces twisting that resists buckling caused by MDF ripple deformations.

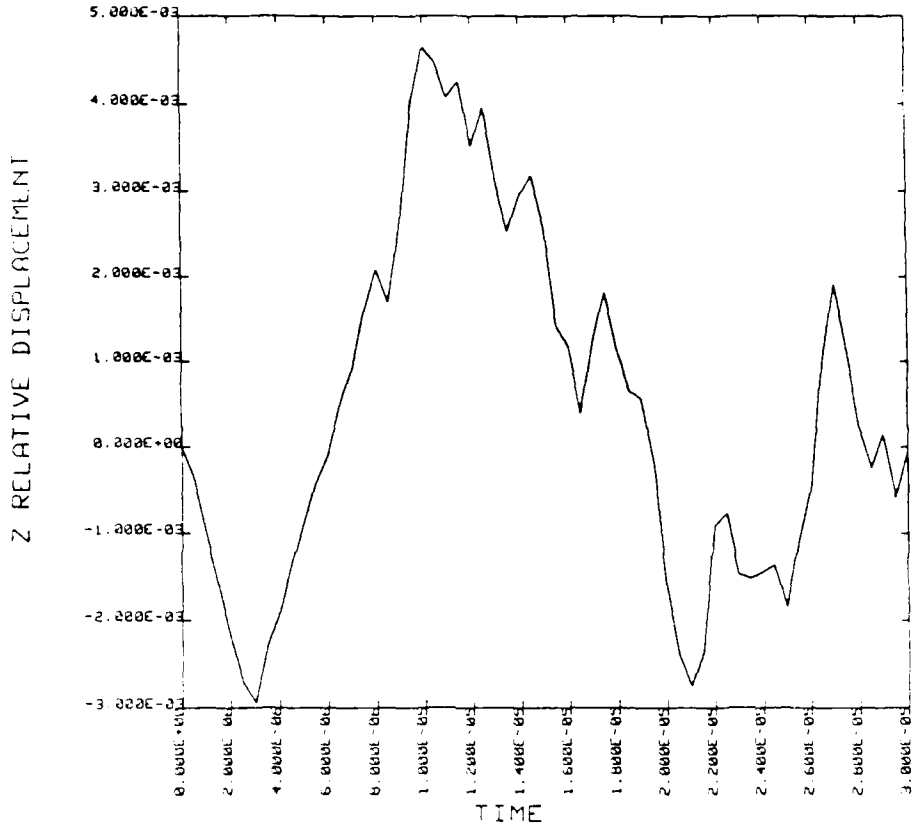

Figure 41. Peak-to-peak deformation from DYNA2D *vs.* time, with 800 taps, $h = 0.762$ mm, $D = 26$ mm, $S_r = 1.6$.

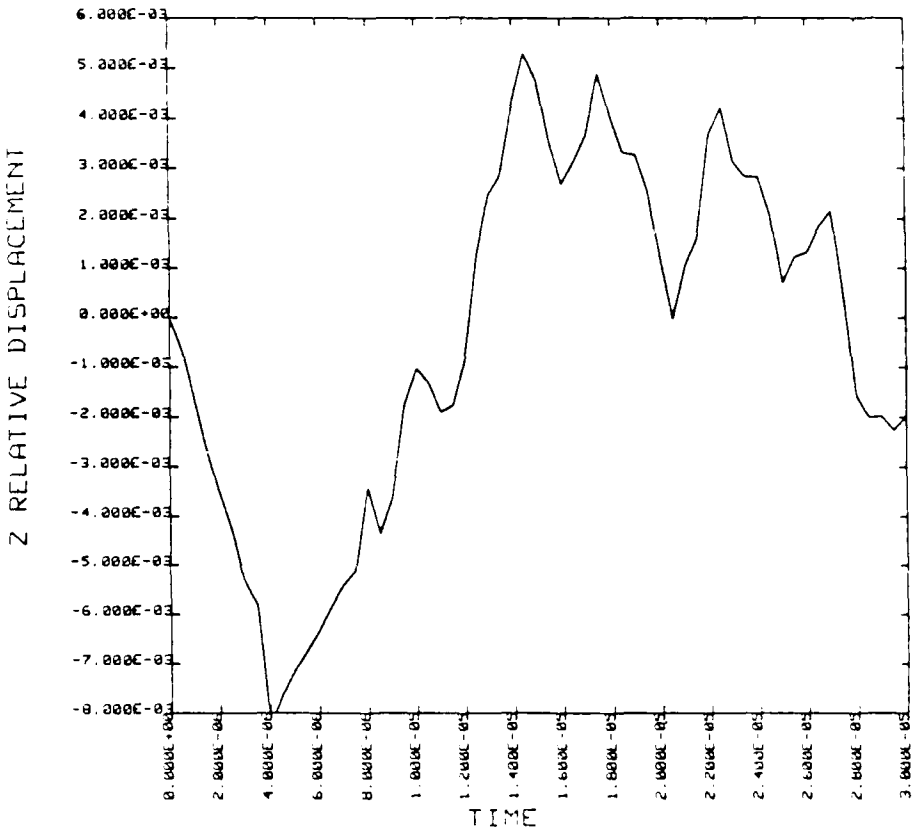

Figure 42. Peak-to-peak deformation from DYNA2D *vs.* time, with 800 taps. $h = 0.762$ mm, $D = 26$ mm, $S_r = 1.0$.

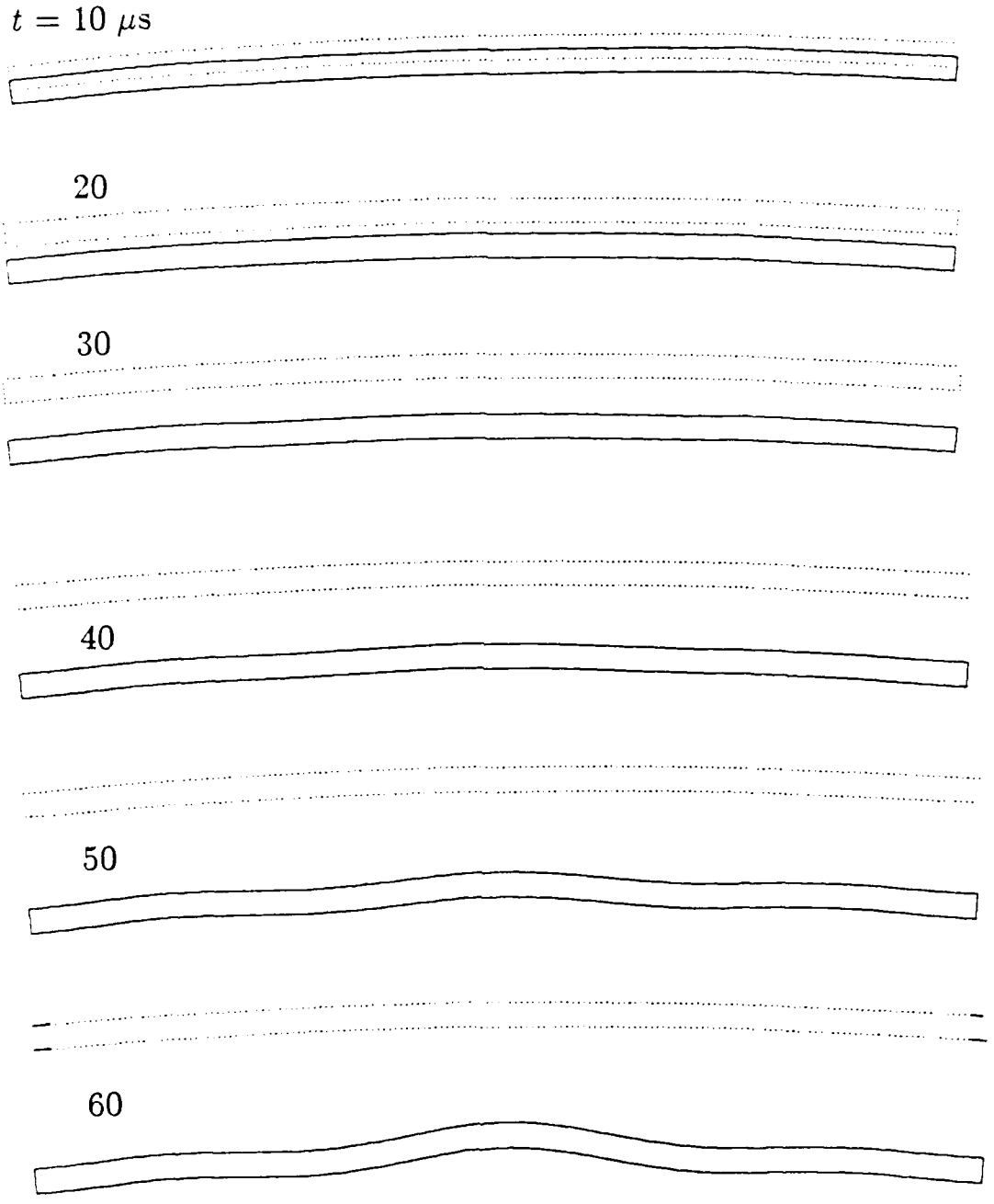

Figure 43. Buckle deformation shapes from DYNA2D with 2100 taps, $h = 0.635$ mm, $D = 26$ mm, $S_r = 2.4$.

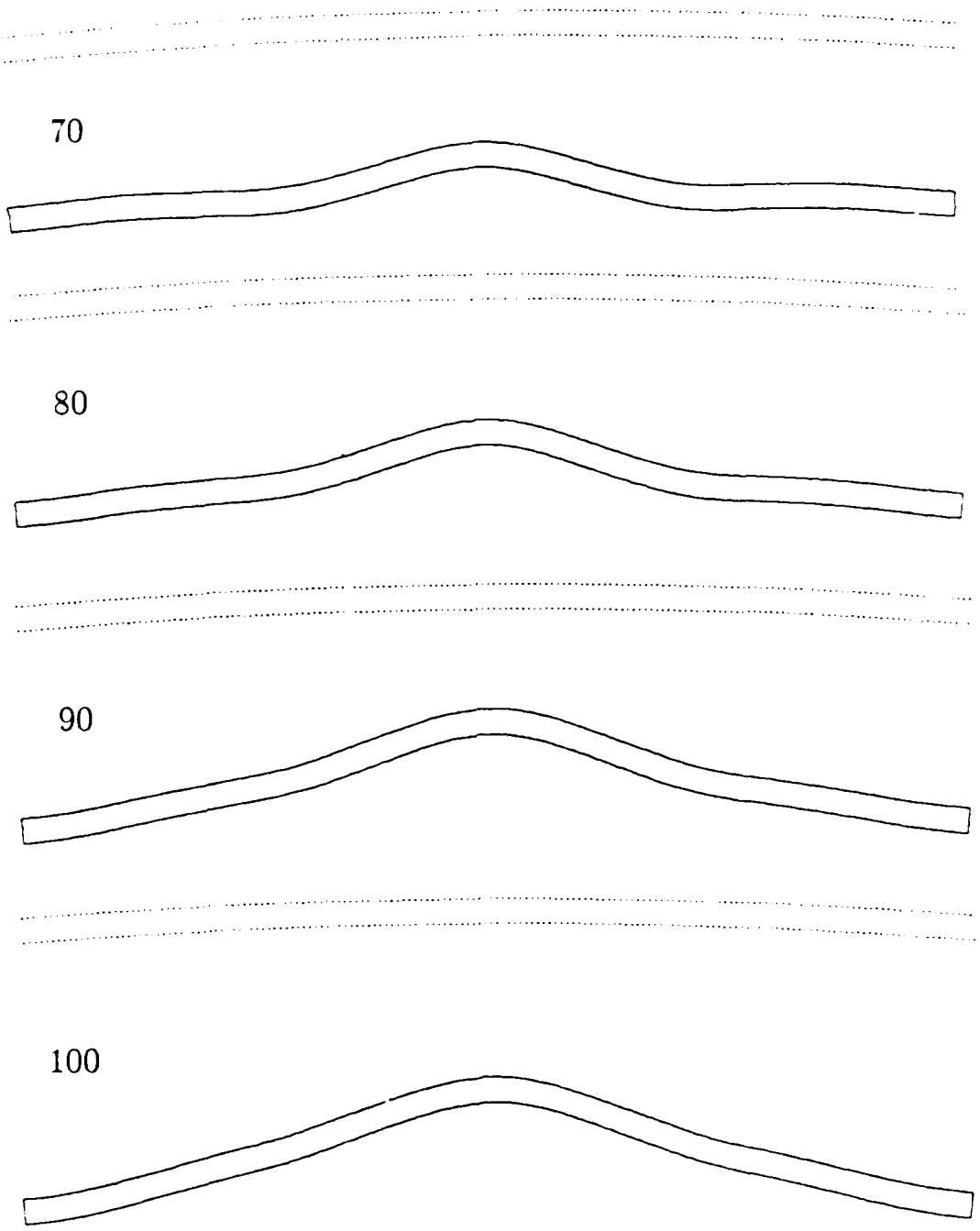

Figure 43. Buckle deformation shapes from DYNA2D with 2100 taps, $h = 0.635$ mm, $D = 26$ mm, $S_r = 2.4$ (concluded).

SECTION 6
LIST OF REFERENCES

1. H. E. Lindberg and Y. D. Murray, *Calibration and Analysis of the SPLAT (Spray Lead at Target) Impulse Simulation Technique*, DNA-TR-81-333, Technical Report, SRI Project 2600, Vol. 3, for Defense Nuclear Agency, November 1983.

2. SRI International *Assessment of the Vulnerability and Lethality of Aerospace Systems, Vol. III: Structural Response of Liquid Fueled Boosters*, Unpublished.

3. R. V. Churchill and J. W. Brown, *Fourier Series and Boundary Value Problems*, Third Edition, McGraw-Hill Book Co., New York, N. Y., 1978.

4. S. W. Kirkpatrick, "Damage to Metal Tanks from Pulsed Flood and Spot Loads," SUBWOG-6P Joint US/UK Workshop, Los Alamos, N. M., February 1986.

5. S. W. Kirkpatrick, P. R. Gefkin and B. S. Holmes, "Update on Liquid Booster Response," LTH-3 Hardening Meeting, Marina del Rey, California, April 1986.

Appendix A
PASCAL PROGRAM FOR PLATE RIPPLE FROM SPLAT

```
{$C-}
Program Riplasci;
{
    Calculates Response of beam to SPLAT loading usine Finite
    Fourier Transforms and integration by Simpson's rule.

    Saves files for use by Shoascii graphics
}
const
  Nmmax = 10;
  Nsmax = 4;
  Ntmax = 100;
  Nx = 40;

type
  vector = array[0..Nx] of real;
var
  Ysave : array[0..Ntmax] of vector;
  XoDsave : vector;
  flag, Ix : Integer;
  Filename : string[30];
  tmaxplus : real;
  Forcepos : array[0..Ntmax,1..Nsmax] of real;
  Forcemag : array[0..Ntmax,1..Nsmax] of real;

  D, Sr, S, v, Vf, h, c, Kcoeff, Q, r : real;
  t, dt, dt2, dt6, dt46, Xi, tmax : real;
  dtmax, dtout, tn, Strandsum, Strandfn, vt, Qrr : real;
  Ntout, tskip, It, It2, Itt, Ittend : integer;
  Is, Im, Nt, Ns, Nm, N : integer;
  omega, K, A, B : array[0..Nmmax] of real;
  Ytrans : array[0..Nmmax,0..Ntmax] of real;
  Astrand : array[1..Nsmax] of real;
  tsave : array[1..Ntmax] of real;
```

```
  Ch : char;
  Done, OK : boolean;

PROCEDURE Namefiles;
BEGIN
  ClrScr;
  Writeln('Give prefix for data files of this run ');
  Write('Prefix: ');
  Readln(Filename);
  Filename := copy(Filename,1,6);
END;

Procedure ModParams;
var
  Paramfile : text;

BEGIN
  ClrScr;
  Writeln('Reading parameter file');
  Assign(Paramfile, 'b:Params.prn');
  Reset(Paramfile);
  Read(Paramfile,Nm,tmax,dt,Sr,v,Vf,c,h,D,dtout);
  Close(Paramfile);
  Done := false;
  WHILE NOT Done DO
    BEGIN
      ClrScr;
      Writeln('Type item number to be changed.');
      Writeln('Hit any other key to begin calculation.');
      Writeln;
      Writeln('1. Number of modes =', Nm:3);
      Writeln('2. Final time (us) =', tmax:7:3);
      Writeln('3. Calculation time step (us) =', dt:8:3);
      Writeln('A. Output time step (us) =     ', dtout:8:3);
      Writeln('4. Standoff ratio =', Sr:7:2);
      Writeln('5. Lead spray velocity (mm/us) = ', v:6:2);
      Writeln('6. Final wall velocity (mm/us) = ', Vf:8:4);
      Writeln('7. Material bar velocity (mm/us) =', c:6:3);
      Writeln('8. Beam thickness (mm) =', h:7:3);
      Writeln('9. Strand spacing (mm) =', D:7:3);
      Writeln;
      IF dtout <> 0 THEN
```

```
  BEGIN
    Writeln('Number of output steps =',
             round(tmax/dtout):4);
    Writeln('Maximum allowable is 100')
  END;
dtmax := (Sqrt(Sr*Sr + 0.0049) - Sr)*D/v;
Writeln;
Writeln('Maximum allowable time step ',
        'for given parameters is dt =',
         dtmax:8:3);
Writeln;
Read(kbd,Ch);
Ch := UpCase(Ch);
CASE Ch OF
  '1' : BEGIN Write(' Number of modes = ');
              Readln(Nm) END;
  '2' : BEGIN Write(' Final time (us) = ');
              Readln(tmax) END;
  '3' : BEGIN Write(' Calculation time step (us) = ');
              Readln(dt) END;
  'A' : BEGIN
          OK := false;
          REPEAT
            Write(' Output time step (us) = ');
            Readln(dtout);
            IF (dt <> 0) AND (dtout > dt) THEN
              BEGIN
                tskip := trunc(dtout/dt);
                Ntout := round(tmax/(dt*tskip));
                Writeln('Number of output steps =',
                         Ntout:4);
                Writeln('Maximum allowable is 100');
                OK := (Ntout <= Ntmax);
              END
            ELSE
              BEGIN
                Writeln('Enter computation ',
                        'step first');
                Read(ch);
                OK := true;
              END;
          UNTIL OK;
```

```
                END;
          '4' : BEGIN Write(' Standoff ratio = ');
                      Readln(Sr) END;
          '5' : BEGIN Write(' Lead spray velocity (mm/us) = ');
                      Readln(v) END;
          '6' : BEGIN Write(' Final wall velocity (mm/us) = ');
                      Readln(Vf) END;
          '7' : BEGIN Write(' Material bar velocity ',
                            '(mm/us) = ');
                      Readln(c) END;
          '8' : BEGIN Write(' Beam thickness (mm) = ');
                      Readln(h) END;
          '9' : BEGIN Write(' Strand Spacing (mm) = ');
                      Readln(D) END;
          ELSE Done := true;
        END; {Case}
      END; {While}
END; {ModParams}

Procedure Parameters;
BEGIN
  S := Sr*D;
  tskip := trunc(dtout/dt);
  Kcoeff := Vf*D*v*S*S/2;
  N := 0;
  tn := 0;
  WHILE tn < tmax DO
    BEGIN
      N := N + 1;
      tn := (Sqrt(N*D*N*D + S*S) - S)/v;
    END;
  Writeln('Active Number of strands on each side =',N:4);
  FOR Is := 1 to N do
      Astrand[Is] := (Is - N)*D;
  FOR Im := 1 to Nm do
    BEGIN
      Omega[Im] := (2*Im*pi/D)*(2*Im*pi/D) * c*h/sqrt(12);
      writeln('Im = ',Im:3, '    Omega = ',Omega[Im]:8:4);
      K[Im] := Kcoeff/omega[Im];
      A[Im] := 0;
      B[Im] := 0;
    END;
```

```
  writeln('dt = ', dt:8:4);
  writeln;
  write('Press ENTER to continue');
  readln(ch);
END;

Procedure FourierCoeff;
BEGIN
  Writeln('Calculating Fourier transform response');
  t := 0;
  It := 0;
  Itt := 0;
  flag := 0;
  tmaxplus := tmax + dt;
  dt2 := 0.05*dt;
  Strandfn := K[Im]*sqrt(2*S*dt2/v + dt2*dt2)/(D*D*D*6);
  Writeln('  t    Itt      Yt2        Yt4        Yt6        Yt8');
  Writeln;
  While t <= tmaxplus do
    BEGIN
      IF Keypressed THEN Halt;
      IF It MOD tskip = 0 THEN
        write(t:4:1, Itt:4);
      A[Im] := A[Im] - Strandfn * sin(Omega[Im]*t);
      B[Im] := B[Im] + Strandfn * cos(Omega[Im]*t);
      IF (t < dt) AND (flag = 0) THEN
        BEGIN
          dt2 := 0.1 * 0.5*dt;
          dt6 := 0.1 * dt/6;
          dt46 := 4*dt6;
          tskip := 10 * trunc(dtout/dt);
          flag := 1;
        END;
      IF (t > dt) AND (flag = 1) THEN
        BEGIN
          dt2 := 0.5*dt;
          dt6 := dt/6;
          dt46 := 4*dt6;
          tskip := trunc(dtout/dt);
          It := 1;
          flag := 0;
        END;
```

```
FOR It2 := 1 to 2 DO
  BEGIN
    t := t + dt2;
    vt := v*t;
    Q := sqrt(2*S*vt + vt*vt);
    r := S + vt;
    Qrr := Q*r*r;
    FOR Im := 1 to Nm do
      BEGIN
        IF (It MOD tskip = 0) AND (It2 = 2) THEN
          BEGIN
            Ytrans[Im,Itt] := 2*(A[Im]*cos(Omega[Im]*t)
                              + B[Im]*sin(Omega[Im]*t));
            IF Im = Nm THEN
              Writeln(Ytrans[Im,Itt]:10:3, Itt:3)
            ELSE Write(Ytrans[Im,Itt]:10:3);
          END;
        Strandsum := 0;
        FOR Is := 1 to N do
          BEGIN
            Xi := Astrand[Is] + Q;
                IF It MOD tskip = 0 THEN
                BEGIN
                  Forcepos[Itt,Is] := Xi/D;
                  Forcemag[Itt,Is] := Kcoeff/Qrr;
                END;
            IF (Xi >= 0) AND (Xi <= D) THEN
                StrandSum := StrandSum
                              + cos(2*Im*pi*Xi/D);
          END; {Strand loop}
        IF It2 = 1 THEN
          Strandfn := K[Im]*Strandsum*dt46/Qrr
          ELSE Strandfn := K[Im]*Strandsum*dt6/Qrr;
        A[Im] := A[Im] - Strandfn * sin(Omega[Im]*t);
        B[Im] := B[Im] + Strandfn * cos(Omega[Im]*t);
      END; {Mode loop}
    END; {Simpson loop}
IF It MOD tskip = 0 THEN
  BEGIN
    IF Itt = 0 then tsave[Itt] := t
    ELSE tsave[Itt] := t - dt;
    Itt := Itt + 1;
```

```
        END;
      It := It + 1;
    END; {t loop}
  Ittend := Itt - 1;
END; {FourierCoeff}

Procedure Saveparams;
var
  Paramfile : text;
  dummy : string[10];
BEGIN
  Writeln('Saving parameter file');
  Assign(Paramfile, 'b:Params.prn');
  Rewrite(Paramfile);
  Write(Paramfile,Nm,tmax,dt,Sr,v,Vf,c,h,D,dtout);
  Str(2*N:4, dummy);
  Write(Paramfile,dummy);
  Close(Paramfile);
END;

Procedure ShoParams;
VAR
  Paramfile : text;
BEGIN
  Writeln('Saving parameters for ShoASCII');
  Assign(Paramfile, 'b:' + Filename + '.prm');
  Rewrite(Paramfile);
  Write(Paramfile, Nm:4, tmax:10:4, dt:10:5, Sr:10:4, v:10:4,
        Vf:10:5, c:10:4, h:10:5, D:10:4, dtout:10:5);
  Close(Paramfile);
END;

Procedure SaveTrans;
var
  Transfile : text;
  time, transform : string[16];

BEGIN
  Writeln('Saving transforms');
  Assign(Transfile, 'b:trans.prn');
  Rewrite(Transfile);
  FOR Itt := 0 to Ittend do
```

```
    BEGIN
      Str(tsave[Itt]:6:2, time);
      Write(Transfile, time);
      FOR Im := 1 to Nm do
        BEGIN
          Str(Ytrans[Im,Itt]:10:6, transform);
          Write(Transfile, transform);
        END;
      Writeln(Transfile);
    END;
  Close(Transfile);
END;

Procedure Shape;

BEGIN {Shape}
  writeln('Ittend = ',Ittend:4);
  Writeln('Calculating deformed shapes');
  FOR Itt := 0 to Ittend do
    BEGIN
      Writeln('Itt =',Itt:3, '    t =', tsave[Itt]:7:3);
      FOR Ix := 0 to Nx do
        BEGIN
          XoDsave[Ix] := Ix/Nx;
          Ysave[Itt,Ix] := 0;
          FOR Im := 1 to Nm do
            BEGIN
              Ysave[Itt,Ix] := Ysave[Itt,Ix] + Ytrans[Im,Itt]
                               *cos(2*Im*pi*XoDsave[Ix]);
            END; {mode loop}
          Ysave[Itt,Ix] := 200*Ysave[Itt,Ix]/(D*h);
        END; {x loop}
    END; {t loop}
END; {Shape}

Procedure SaveShape;

VAR  Timefile : text;
     Shapefile : text;

BEGIN
  Writeln('Saving deformed shapes');
```

```
  Assign(Shapefile, 'b:' + Filename + '.shp');
  Rewrite(Shapefile);
  For Ix := 0 to Nx DO
    Write(Shapefile, XoDsave[Ix]:9:4);
  FOR Itt := 0 to Ittend DO
    FOR Ix := 0 to Nx DO
      Write(Shapefile,Ysave[Itt,Ix]:10:3);
  Close(Shapefile);

  Assign(Timefile, 'b:' + Filename + '.tim');
  Rewrite(Timefile);
  Write(Timefile,Ittend);
  FOR Itt := 0 to Ittend DO
    Write(Timefile,tsave[Itt]:9:4);
  Close(Timefile);
END;

PROCEDURE SaveForces;

VAR Forcefile : Text;
    Itime, Istrand : integer;

BEGIN
  Writeln('Saving Forces');
  Assign(Forcefile,'b:' + filename + '.frc');
  Rewrite(Forcefile);
  Write(forcefile, Ittend:5);
  Write(forcefile, N:5);
  FOR Itime := 0 to Ittend DO
    FOR Istrand := 1 to N DO
      write(Forcefile, Forcepos[Itime,Istrand]:10:4,
                       Forcemag[Itime,Istrand]:10:4);
  Close(Forcefile);
END;


BEGIN {MainProgram}
  NameFiles;
  ModParams;
  Parameters;
  FourierCoeff;
  Saveparams;
```

```
  Shoparams;
  Shape;
  SaveShape;
  SaveForces;
END.
```

Appendix B
PASCAL PROGRAM FOR INTERACTIVE GRAPHIC DISPLAY

```
{$C-}
PROGRAM Shoascii;

{Displays ripple shapes from Riplasci
 shape files in ASCII format}

{$I c:Graph.p }
{This is the Turbo Pascal graphics programs file}

TYPE vector = array[0..40] of real;
     name = string[60];

VAR  x : vector;
     y : ARRAY [0..100] of vector;
     time : ARRAY[0..100] of real;
     i, j, jcurve, indexIncrement, Mpoints, Ncurves,
       Nforces : integer;
     A, B, phase : real;
     Tx, Ty, Tg : name;
     Signoff, ch, boxtype : char;
     OK, firstbox : boolean;
     Filename : string[30];
     Forcepos : array[0..100,1..4] of real;
     Forcemag : array[0..100,1..4] of real;

PROCEDURE Namefiles;
BEGIN
  ClrScr;
  Writeln('Give prefix for data files of this run. ');
  Write('Prefix: ');
  Readln(Filename);
  Filename := copy(Filename,1,6);
  Writeln(Filename);
END;
```

```
Procedure ShoParams;
var
  Paramfile : text;
  Nm : integer;
  tmax,dt,Sr,v,Vf,c,h,D,dtout : real;

BEGIN
  ClrScr;
  Writeln('Reading parameter file');
  Assign(Paramfile, 'b:' + Filename + '.prm');
  Reset(Paramfile);
  Read(Paramfile,Nm,tmax,dt,Sr,v,Vf,c,h,D,dtout);
  Close(Paramfile);
  Writeln('Parameters for these plots are:');
  Writeln;
  Writeln('1. Number of modes =', Nm:3);
  Writeln('2. Final time (us) =', tmax:7:3);
  Writeln('3. Calculation time step (us) =', dt:8:3);
  Writeln('A. Output time step (us) =     ', dtout:8:3);
  Writeln('4. Standoff ratio =', Sr:7:2);
  Writeln('5. Lead spray velocity (mm/us) = ', v:6:2);
  Writeln('6. Final wall velocity (mm/us) = ', Vf:8:4);
  Writeln('7. Material bar velocity (mm/us) =', c:6:3);
  Writeln('8. Beam thickness (mm) =', h:7:3);
  Writeln('9. Strand spacing (mm) =', D:7:3);
  Writeln;
  Writeln('Hit any key but Q to begin input and
           plot program.');
  Writeln;  Writeln('Hit Q to terminate program.');
  Read(kbd,ch);
  IF UpCase(ch) = 'Q' THEN HALT;
END;

PROCEDURE Plotxy(VAR x,y : vector; gridX, npoints : integer;
                 Tx,Ty,Tg : name);

{ Creates x,y plots with automatic grid generation
  with tics in multiples of 1, 2, or 5, according
  to range of y variable}

CONST  screenX = 639;  screenY = 199;
```

```
        eight = 8;  ten = 10;  twelve = 12; fourteen = 14;
        half = 0.5; one = 1;  two = 2;  four = 4;
        ytic = 5; xtic = 10; white = 1; leftborder = 51;
        topborder = 10; bottomborder = 174;
        rightborder = 622;

VAR  exp, printcount, gridY : integer;
     i, nx, ny, nxo, nyo : integer;
     xticloc, yticloc, ticseparation, topinbord,
       botinbord, leftinbord,
       rightinbord, boxX, boxY : integer;
     normmin, min, max, delX, delY, E, ylabel, EdelY,
       range, Xscale, Yscale, offset, Xmin, Xmax : real;
     ch : char;
     charbuf : string[80];
     MonitorType : byte absolute $0000:$0410;

PROCEDURE Minmax;

BEGIN
  min := y[0];
  max := y[0];
  FOR i := 1 to npoints DO
    BEGIN
      IF y[i] < min
        THEN min := y[i]
        ELSE IF y[i] > max
          THEN max := y[i]
    END;
  range := max - min;
  Xmin := x[0];
  Xmax := x[npoints];
  delX := (Xmax - Xmin)/gridX;
END;

PROCEDURE Grid;

BEGIN
  IF range = 0 THEN
    BEGIN
      MonitorType := MonitorType OR $30;
      Textmode(bw80);
```

```
    GoToXY(1,1);
    writeln('Bad input; zero y range');
    halt;
  END;
E := 1;
exp := 0;
REPEAT
  IF range < 3.5
    THEN
      BEGIN
        range := ten * range;
        E := E/ten;
        exp := exp - 1;
      END
    ELSE IF range > 36
      THEN
        BEGIN
          range := range/ten;
          E := E * ten;
          exp := exp + 1
        END;
UNTIL (range >= 3.5) and (range <= 36);
normmin := min/E;
IF range <= 3.5
  THEN BEGIN gridY := eight; delY := half  END
  ELSE IF range < 4.5
    THEN BEGIN gridY := ten; delY := half  END
  ELSE IF range < 5.5
    THEN BEGIN gridY := twelve; delY := half  END
  ELSE IF range < 6.5
    THEN BEGIN gridY := fourteen; delY := half  END
  ELSE IF range < 7
    THEN BEGIN gridY := eight; delY := one  END
  ELSE IF range < 9
    THEN BEGIN gridY := ten; delY := one  END
  ELSE IF range < 11
    THEN BEGIN gridY := twelve; delY := one  END
  ELSE IF range < 13
    THEN BEGIN gridY := fourteen; delY := one  END
  ELSE IF range < 14
    THEN BEGIN gridY := eight; delY := two  END
  ELSE IF range < 18
```

```
      THEN BEGIN gridY := ten; delY := two  END
    ELSE IF range < 22
      THEN BEGIN gridY := twelve; delY := two  END
    ELSE IF range < 26
      THEN BEGIN gridY := fourteen; delY := two  END
    ELSE IF range < 28
      THEN BEGIN gridY := eight; delY := four  END
      ELSE BEGIN gridY := ten; delY := four  END;
  END; {Grid}

PROCEDURE TextScreen;
  BEGIN
    MonitorType := MonitorType OR $30;
    Textmode(bw80);
    GoToXY(1,1);
  END;

PROCEDURE GraphScreen;
  BEGIN
    MonitorType := (MonitorType AND $CF) OR $10;
    IF boxtype = 'S' THEN
      BEGIN
        GraphWindow(53,15,620,169);
        FillScreen(0);
        GraphWindow(0,0,639,199);
      END
    ELSE IF boxtype <> 'A' THEN HiRes;
  END;

PROCEDURE Boxantic;

BEGIN
  Draw(leftborder,topborder,rightborder,
       topborder,white);                    {top}
  Draw(leftborder,bottomborder,rightborder,
       bottomborder,white);                 {bottom}
  Draw(leftborder,topborder,leftborder,
       bottomborder,white);                 {left}
  Draw(rightborder,topborder,rightborder,
       bottomborder,white);                 {right}
  topinbord := topborder + ytic;
  botinbord := bottomborder - ytic;
```

```
    leftinbord := leftborder + xtic;
    rightinbord := rightborder - xtic;
    boxX := rightborder - leftborder;
    boxY := bottomborder - topborder;
    FOR i := 1 to gridX - 1  DO {top and bottom tics}
      BEGIN
        xticloc := leftborder + Round(i * boxX/gridX);
        Draw(xticloc,topborder,xticloc,topinbord,white);
        Draw(xticloc,bottomborder,xticloc,botinbord,white);
      END;
    FOR i := 1 to gridY - 1  DO {left and right tics}
      BEGIN
        yticloc := bottomborder - Round(i * boxY/gridY);
        Draw(leftborder,yticloc,leftinbord,yticloc,white);
        Draw(rightborder,yticloc,rightinbord,yticloc,white);
      END;
  END; {Boxantic}

  PROCEDURE Gridnumbers;

  BEGIN
    IF normmin < 0 THEN
      ylabel := (trunc((normmin - 0.2)/delY) - 1) * delY
      ELSE ylabel := trunc((normmin - 0.2)/delY) * delY;
    FOR i := 0 to gridY  DO
      BEGIN
        gotoXY(1,1);
        IF delY = half THEN
          write(ylabel:4:1)
          ELSE write(ylabel:4:0);
        ylabel := ylabel + delY;
        GetPic(charbuf,0,0,31,7);
        If i = gridY THEN
          BEGIN  gotoXY(1,1);
                 write('     ')   END;
        yticloc := bottomborder - Round(i * boxY/gridY) + 4;
        PutPic(charbuf,16,yticloc);
      END;
  END; {Gridnumbers}

  PROCEDURE Xgridnumbers;
```

```
var xlabel : real;
    xticloc : integer;

BEGIN
  FOR i := 0 to gridX DO
  BEGIN
    gotoXY(1,1);
    xlabel := (i*delX);
    write(xlabel:5:1);
    GetPic(charbuf,0,0,38,7);
    xticloc := leftborder + Round(i * boxX/gridX) - 28;
    PutPic(charbuf,xticloc,bottomborder + 13);
  END;
END; {Xgridnumbers}

PROCEDURE Titles;

var  Ytitlelen, start : integer;
     expchar : string[2];

BEGIN

  gotoXY(42 - Length(Tx) div 2, 25);
  write(Tx);
  gotoXY(42 - Length(Tg) div 2, 1);
  write(Tg);
  Str(exp:2, expchar);
  Ty := Copy(Ty,1,18);
  Ty := Ty + '  E' + expchar;
  Ytitlelen := Length(Ty);
  start := 12 - Ytitlelen div 2;
  FOR i := 1 to Ytitlelen DO
    BEGIN
    gotoXY(1,start + i);
    write(copy(Ty,i,1));
    END;
END;

PROCEDURE Plot;

VAR Forcelength, Forceposition, LeftforceX,
    RightforceX, j : integer;
```

```
BEGIN

  IF min < 0
    THEN offset := delY * (trunc((-normmin
                  + 0.2) / delY) + 1) * E
    ELSE offset := delY * trunc((-normmin
                  + 0.2) / delY) * E;
  Xscale := boxX / (Xmax - Xmin);
  Yscale := boxY / (gridY * delY * E);
  nxo := leftborder + trunc((x[0] - Xmin) * Xscale);
  nyo := bottomborder - trunc((y[0] + offset) * Yscale);
  FOR i := 1 to npoints DO
    BEGIN
      nx := leftborder + trunc((x[i] - Xmin) * Xscale);
      ny := bottomborder - trunc((y[i] + offset) * Yscale);
      draw(nxo,nyo,nx,ny,white);
      nxo := nx;   nyo := ny;
    END;
  FOR i := 1 to Nforces DO
    BEGIN
      IF (Forcepos[jcurve,i] > 0) AND
         (Forcepos[jcurve,i] < 1) THEN
      BEGIN
        Forcelength := trunc((Forcemag[jcurve,i]
                      /Forcemag[1,1])*100);
        Forceposition := trunc(Forcepos[jcurve,i] * boxX);
        LeftforceX := leftborder + Forceposition;
        RightforceX := Rightborder - Forceposition;
        Draw(LeftforceX,150,LeftforceX,150
             - Forcelength,white);
        Draw(LeftforceX+1,150,LeftforceX+1,150
             - Forcelength,white);
        Draw(RightforceX,150,RightforceX,150
             - Forcelength,white);
        FOR j := 1 to Nforces + 1 - i DO
          draw(rightborder-60,topborder+10+2*j,
               rightborder-50,topborder+10+2*j,white);
      END;
    END;
END; {plot}
```

```
BEGIN {Plotxy}
  GraphScreen;
  IF (boxtype <> 'A') AND (boxtype <> 'S') THEN
    BEGIN
      Minmax;
      Grid;
      Boxantic;
      Xgridnumbers;
      Gridnumbers;
      Titles;
    END;
  Plot;
  TextScreen;
END;

PROCEDURE GraphType;

BEGIN
    ClrScr;
    Writeln;
    Writeln('Enter Graph type: ',
            'A = add plot to existing grid');
    Writeln('                  ',
            'S = subsitute plot onto existing grid');
    Writeln('                  Q = quit program');
    Writeln('Any other entry gives new plot on new grid');
    Writeln;
    Write('Graph Type = ');
    Readln(boxtype);
    boxtype := UpCase(boxtype);
    IF firstbox THEN
      BEGIN
        boxtype := 'N';
        firstbox := false END;
END;

PROCEDURE Readcurves;

VAR  Timefile : text;
     Shapefile : text;
     Ix : integer;
```

```
CONST Nx = 40;

BEGIN
  Writeln;
  Writeln('Reading times and shapes');
  Assign(Timefile, 'b:' + Filename + '.tim');
  Reset(Timefile);
  Read(Timefile, Ncurves);
  FOR i := 0 to Ncurves DO
    Read(Timefile, time[i]);
  Close(Timefile);

  Assign(Shapefile,'b:' + Filename + '.shp');
  Reset(Shapefile);
  FOR Ix := 0 to Nx DO
    Read(Shapefile, x[Ix]);
  FOR j := 0 to ncurves DO
    FOR Ix := 0 to Nx DO
      Read(Shapefile, y[j,Ix]);
  Close(Shapefile);
END;

PROCEDURE readforces;

VAR forcefile : text;
    it, ix, Ittend : integer;
    ch :char;

BEGIN
  Writeln('Reading forces');
  Assign(forcefile, 'b:' + Filename + '.frc');
  Reset(forcefile);
  Read(forcefile, Ittend);
  Read(forcefile, Nforces);
  Writeln;
  Writeln('Active number of strands =',Nforces:3);
  FOR it := 0 to Ittend DO
    FOR ix := 1 to Nforces DO
      Read(forcefile, Forcepos[It,Ix], Forcemag[It,Ix]);
  Close(Forcefile);
END;
```

```
BEGIN {Shoshape}
Signoff := 'A';
REPEAT
ClrScr;
Writeln('Enter Q to quit, any other character to go again');
Read(Signoff);
If UpCase(Signoff) = 'Q' THEN halt;
Namefiles;
ShoParams;
Readforces;
Tx := 'Distance Between Strands, x/D';
Ty := '% WALL THICKNESS';
Tg := 'RIPPLE DEFORMATION BETWEEN STRANDS';
A := 1;
B := 0;
Mpoints := 40;
Readcurves;
firstbox := true;
boxtype := 'N';
jcurve := 0;
WHILE boxtype <> 'Q' DO
  BEGIN
    IF (jcurve < 1) OR (jcurve > Ncurves) THEN GraphType;
    ClrScr;
    IF boxtype <> 'Q' THEN
    BEGIN
    Case boxtype OF
      'S' : Writeln('SUBSTITUTING PLOT ONTO EXISTING GRID');
      'A' : Writeln('ADDING PLOT TO EXISTING ',
                    'PLOTS AND GRID ');
      ELSE  Writeln('CREATING A NEW GRID AND ',
                    'PLOTTING BASE CURVE'); END;
    Writeln('(To change plot mode,');
    Writeln(' enter a letter or plot index ',
            'outside of range.)');
      Writeln;
      Writeln('Index range for current plots is 1 to',
              Ncurves:4);
      Writeln('Current index value is',jcurve:3);
      Writeln('Current time is ',time[jcurve]:5:2,
              ' microseconds');
      Write('Enter curve index increment: ');
```

```
      {$I-} readln(indexIncrement) {$I+} ;
      OK := (IOresult = 0);
      IF not OK then jcurve := 0
        ELSE
        jcurve := jcurve + indexIncrement;
    IF (jcurve > 0) AND (jcurve <= Ncurves) THEN
      Plotxy(x,y[jcurve],10,Mpoints,Tx,Ty,Tg);
    END; {IF boxtype}
  END;
UNTIL Signoff = 'Q';
END.
```

DISTRIBUTION LIST

DEPARTMENT OF DEFENSE

DEFENSE ADVANCED RSCH PROJ AGENCY
ATTN: F PATTEN

DEFENSE INTELLIGENCE AGENCY
ATTN: G WEBER
ATTN: RTS-2B

DEFENSE NUCLEAR AGENCY
ATTN: SPLH
ATTN: SPWE
4 CYS ATTN: TITL

DEFENSE TECHNICAL INFORMATION CENTER
12 CYS ATTN: DD

STRATEGIC DEFENSE INITIATIVE ORGANIZATION
ATTN: R YESENSKY
ATTN: P TERRY
ATTN: S GEARY

UNDER SECRETARY OF DEFENSE
ATTN: ENGR TECH J PERSCH

DEPARTMENT OF THE ARMY

U S ARMY MATERIAL TECHNOLOGY LABORATORY
ATTN: R FITZPATRICK

U S ARMY MISSILE COMMAND
ATTN: H GREENE

U S ARMY STRATEGIC DEFENSE COMMAND
ATTN: F SAVAGE
ATTN: S BROCKWAY

DEPARTMENT OF THE NAVY

NAVAL INTELLIGENCE SUPPORT CTR
ATTN: A COBLEIGH

NAVAL POSTGRADUATE SCHOOL
ATTN: PROF K E WOEHLER, CODE 61WH

NAVAL RESEARCH LABORATORY
ATTN: CODE 4600 D NAGEL
ATTN: CODE 4633 R WENZEL

NAVAL SEA SYSTEMS COMMAND
2 CYS ATTN: PMS

NAVAL SURFACE WEAPONS CENTER
ATTN: CODE R-31 J THOMPSON

OFFICE OF NAVAL TECHNOLOGY
ATTN: CODE 217

STRATEGIC SYSTEMS PROGRAM OFFICE (PM-1)
ATTN: NSP-L63 (TECH LIB)

DEPARTMENT OF THE AIR FORCE

AIR FORCE CTR FOR STUDIES & ANALYSIS
ATTN: AFCSA/SAMI (R GRIFFIN)

AIR FORCE SYSTEMS COMMAND
ATTN: DLWM

AIR FORCE WEAPONS LABORATORY
ATTN: NTCO C AEBY
ATTN: B FREDERICKSON
ATTN: E HERRERA
ATTN: J WALTON
ATTN: T EDWARDS

AIR FORCE WRIGHT AERONAUTICAL LAB
ATTN: W WOODY
ATTN: B LAINE
ATTN: J RHODEHAMEL
ATTN: S R LYON
ATTN: W HARRIS

FOREIGN TECHNOLOGY DIVISION, AFSC
ATTN: A CORDOVA

DEPARTMENT OF ENERGY

EG&G IDAHO INC
ATTN: J EPSTEIN

LAWRENCE LIVERMORE NATIONAL LAB
ATTN: F SERDUKE
ATTN: W BOOKLESS
ATTN: H KRUGER
ATTN: M GERASSIMENRO

LOS ALAMOS NATIONAL LABORATORY
ATTN: A GREENE
ATTN: T KING
ATTN: R S DINGUS
ATTN: J PORTER

SANDIA NATIONAL LABORATORIES
ATTN: A MCDONALD
ATTN: M BIRNBAUM

SANDIA NATIONAL LABORATORIES
ATTN: DR J POWELL
ATTN: K MATZEN

DEPARTMENT OF DEFENSE CONTRACTORS

ACUREX CORP
ATTN: B LAUB

AEROSPACE CORP
ATTN: H BLAES
ATTN: R COOPER
ATTN: T PARK

APTEK, INC
ATTN: DR E FITZGERALD

APTEK, INC
2 CYS ATTN: H E LINDBERG

BATTELLE MEMORIAL INSTITUTE
ATTN: C WALTERS

GENERAL ELECTRIC CO
ATTN: D ENLOW

GENERAL RESEARCH CORP
ATTN: R PARISSE

GENERAL RESEARCH CORP
ATTN: J SOMMERS

JAYCOR
ATTN: P SCHALL

KAMAN SCIENCES CORP
ATTN: J CARPENTER
ATTN: R ALMASSY

KAMAN SCIENCES CORPORATION
2 CYS ATTN: DASIAC

KAMAN TEMPO
ATTN: DASIAC

KTECH CORP
ATTN: D KELLER

LOCKHEED MISSILES & SPACE CO, INC
ATTN: J PEREZ

MARTIN MARIETTA DENVER AEROSPACE
ATTN: E FRIEDMAN

MCDONNELL DOUGLAS CORP
ATTN: D JOHNSON
ATTN: J S KIRBY
ATTN: L COHEN

PACIFIC-SIERRA RESEARCH CORP
ATTN: H BRODE, CHAIRMAN SAGE

PHYSICAL SCIENCES, INC
ATTN: A PIRRI

PHYSICS INTERNATIONAL CO
ATTN: M KRISHNAN

R & D ASSOCIATES
ATTN: B GOULD
ATTN: D GAKENHEIMER
ATTN: F A FIELD
ATTN: P A MILES

RAND CORP
ATTN: E HARRIS

S-CUBED
ATTN: G GURTMAN

SCIENCE APPLICATIONS INTL CORP
ATTN: E TOTON
ATTN: R AIREY
ATTN: S METH
ATTN: W CHADSEY

SCIENCE APPLICATIONS INTL CORP
ATTN: T LAGANELLI

SCIENCE APPLICATIONS INTL CORP
ATTN: H JANEE

SPARTA, INC
ATTN: J E LOWDER
ATTN: R G ROOT

SRI INTERNATIONAL
ATTN: B HOLMES
ATTN: D CURRAN
ATTN: G ABRAHAMSON

TRW ELECTRONICS & DEFENSE SECTOR
ATTN: W POLICH

TRW INC
ATTN: F FENDELL
ATTN: I RUBIN
ATTN: M SEIZEW

VERAC, INC
ATTN: P CARLSON
ATTN: R BINKOWSKI

W J SCHAFER ASSOCIATES, INC
ATTN: J REILLY

END

DATE

FILMED

5 — 88

DTIC